

R2 priors for Grouped Variance Decomposition in High-dimensional Regression

Javier Enrique Aguilar^{*,†}, David Kohns[†], Aki Vehtari[†] and Paul-Christian Bürkner^{*}

Abstract.

We introduce the Group-R2 decomposition prior, a hierarchical shrinkage prior that extends R2-based priors to structured regression settings with known groups of predictors. By decomposing the prior distribution of the coefficient of determination R^2 in two stages, first across groups, then within groups, the prior enables interpretable control over model complexity and sparsity. We derive theoretical properties of the prior, including marginal distributions of coefficients, tail behavior, and connections to effective model complexity. Through simulation studies, we evaluate the conditions under which grouping improves predictive performance and parameter recovery compared to priors that do not account for groups. Our results provide practical guidance for prior specification and highlight both the strengths and limitations of incorporating grouping into R2-based shrinkage priors.

Keywords: Prior specification, shrinkage priors, variance decomposition, regularization.

1 Introduction

In regression problems involving high-dimensional or structured predictors, it is common for covariates to exhibit natural groupings. These groupings often reflect underlying scientific structure. For example, genes in the same biological pathway (Li and Li, 2008; Sun et al., 2014), indicators of socioeconomic time-series (Kohns and Potjagailo, 2025), or survey items that measure the same latent construct (Bentler and Bonett, 1980). In such cases, incorporating group structure into the prior distribution can improve estimation, interpretability, and predictive performance. However, many existing group-aware priors are motivated by marginal shrinkage properties and offer limited control over interpretable model summaries, such as the proportion of variance explained.

The coefficient of determination, R^2 , is one such interpretable quantity which summarizes how well the model fits the data and is considered to be understood in many applied fields (Gelman et al., 2013). Shrinkage priors built around a prior distribution on R^2 , such as the R2D2 prior and its extensions, allow users to express beliefs about model complexity and sparsity (Zhang et al., 2020; Aguilar and Bürkner, 2023; Yanchenko et al., 2025a; Kohns et al., 2025; Aguilar and Bürkner, 2025). As R2-type priors start from defining the prior distribution on R^2 , they are predictively consistent priors. This means

^{*}TU Dortmund

[†]Aalto University

[‡]Corresponding author: javier.aguilarr@icloud.com url: <https://jea2412.github.io>

that the prior predictive distribution does not substantially change when more model components are added. However, R2-based priors typically assume exchangeability across coefficients and do not consider structural information such as grouping. This can be suboptimal for parameter inference as well as prediction in structured regression settings where variance is expected to concentrate in specific subsets of predictors. Correct allocation of variance matters for both for parameter recovery and prediction.

In this work, we introduce the Group-R2 prior, a class of continuous shrinkage priors that generalizes the R2-based framework to explicitly account for known grouping structures among predictors. Our approach builds on the idea of decomposing the total prior variance implied by an R^2 distribution, and extends it through a two-stage hierarchical allocation: first, the total variance is distributed across groups, and then within each group across individual coefficients. This leads to a prior that allows for targeted control over sparsity and signal dispersion at both the group and coefficient levels.

We show that Group-R2 prior retains the desirable properties of global-local shrinkage priors, including heavy-tailed marginals, concentration at zero, and robustness to large signals. We additionally show how the shrinkage behavior of the prior depends on a small number of interpretable hyperparameters, and we propose strategies for setting them based on theoretical and shrinkage properties. These influence a measure of implicit model sizes, which the user can use to tune the prior. Many previous approaches to setting priors on known groups of coefficients have been similarly motivated from the global-local class of priors for exchangeable coefficients (Xu and Ghosh, 2015; Xu et al., 2016; Boss et al., 2023). However, only the Group Inverse-Gamma Gamma (GIGG) prior of Boss et al. (2023) similarly regularize via three scales in the prior: a global, common to all coefficients, a group-wise scale shared by all members of a group, and one individual to each coefficient. We therefore consider the GIGG prior the main benchmark to the Group-R2¹.

We conduct simulation studies to evaluate the performance of the prior. We additionally seek to understand whether incorporating grouping information into the prior meaningfully improves inference, and under what conditions. To this end, we compare grouped and nongrouped versions of the R2 prior across a range of controlled scenarios that vary in signal strength, sparsity pattern, and dimensionality. These simulations allow us to isolate the effect of the additional decomposition structure and assess its impact on predictive performance, parameter recovery, and shrinkage behavior. We provide empirical evidence on when grouping helps and when it does not.

2 Methods

In this section, we develop the Group-R2 prior, a hierarchical shrinkage prior that decomposes explained variance across and within predictor groups. We begin by detailing the construction of the prior in Section 2.1. We then present related priors in the

¹Many competing group-global local priors have been compared in Boss et al. (2023), we refer the reader to this paper for an excellent overview .

literature that also account for grouped structures in Section 2.2. We introduce the concept of group-wise explained variance and related quantities in Section 2.3. We then derive key theoretical properties, including marginal and joint distributions, behavior near the origin and in the tails, and implications for shrinkage at both the group and coefficient levels in Section 2.4. We analyze the shrinkage behavior induced by the prior through the study of shrinkage factors and the effective number of non-zero coefficients in Section 2.5, and provide practical recommendations for hyperparameter specification in Section 2.6.

2.1 Group-R2 Decomposition priors

Our main interest lies in performing inference for the linear regression model in a situation in which the user already has knowledge about relevant groups of predictors. We will use the available group information to construct a multivariate continuous joint shrinkage prior that accounts for the grouping structures through the variance. Importantly, we do not assume the user has information about the dependency structure within the groups, only about which predictors belong to each mutually exclusive group (Müller and Quintana, 2004).

Let y denote the vector of n observations $(y_1, \dots, y_n)'$, and let X be the design matrix of dimension $n \times p$. Suppose that we have prior knowledge of G groups. For each group $g = 1, \dots, G$, let X_g be the matrix of predictors for that group, of dimension $n \times p_g$, where p_g denotes the column dimension of the g th group, and let the corresponding regression coefficients be $b_g = (b_{g1}, \dots, b_{gp_g})'$. The overall design matrix can be written as $X = (X_1 \dots X_G)$, with associated coefficient vector $b = (b_1' \dots b_G')'$. The linear regression model under consideration is

$$y = b_0 J + \sum_{g=1}^G X_g b_g + \varepsilon, \quad (1)$$

where J is a vector of ones, $b_0 \in \mathbb{R}$ is the intercept and $\varepsilon = (\varepsilon_1 \dots \varepsilon_n)'$ is such that $\varepsilon_i \sim \mathcal{N}(0, \sigma^2)$.

This model can be equivalently expressed observation-wise as

$$y_i = b_0 + \sum_{g=1}^G \sum_{j=1}^{p_g} x_{ij} b_j \mathbf{1}_{\{j=g\}} + \varepsilon_i, \quad i = 1, \dots, n, \quad (2)$$

where $\mathbf{1}$ is the indicator function. Priors that decompose the proportion of explained variance R^2 first define a global R^2 measure, which is then related to the variance of the linear predictor $x'b$ via a one-to-one transformation. Consequently, probabilistic statements about R^2 directly translate to statements about the total variance. This total variance is subsequently decomposed to determine the scales of the coefficients b using an appropriate distribution, such as a normal or double exponential, to express the variability attributed to these coefficients.

We begin by defining the global R^2 measure as

$$R^2 := \text{Cor}^2(y, x'b) = \frac{\text{Var}(x'b)}{\text{Var}(x'b) + \sigma^2}. \quad (3)$$

In the following assume that $\mathbb{E}(x) = 0$ and $\text{Var}(x) = \Sigma_x$, where Σ_x has a diagonal of ones. We further assume the prior for b satisfies $\mathbb{E}(b) = 0$ and $\text{Var}(b) = \sigma^2 \Lambda$, with Λ being a diagonal matrix whose entries are $\lambda_1^2, \dots, \lambda_p^2$. Calculating the variance of the linear predictor yields $\text{Var}(x'b) = \sigma^2 \sum_{i=1}^p \lambda_i^2$. The quantity $\tau^2 := \sum_{i=1}^p \lambda_i^2$ is denoted as the total variance. This implies the following one-to-one relationship between R^2 and τ^2

$$R^2 = \frac{\tau^2}{\tau^2 + 1}. \quad (4)$$

Therefore probabilistic statements about the proportion of explained variance R^2 can be translated to the total variance τ^2 and vice versa. To incorporate group structures, we further decompose Λ into a block-diagonal matrix with entries $\Lambda_1, \dots, \Lambda_G$, where $\Lambda_g = \text{diag}(\lambda_{g1}^2, \dots, \lambda_{gp_g}^2)$. We can rewrite the total variance τ^2 as

$$\tau^2 = \sum_{g=1}^G \sum_{l=1}^{p_g} \lambda_{gl}^2 = \sum_{g=1}^G \tau_g^2, \quad (5)$$

where $\tau_g^2 = \sum_{l=1}^{p_g} \lambda_{gl}^2$ represents the explained variance attributable to the g th group. We construct the Group R^2 prior through the following two-stage decomposition:

Stage I: Group variance decomposition. Decompose the total variance τ^2 across groups using groupwise proportions $\phi = (\phi_1, \dots, \phi_G)$ such that $\phi_g \geq 0$ and $\sum_{g=1}^G \phi_g = 1$. The variance contribution of each group is then $\tau_g^2 = \phi_g \tau^2$.

Stage II: Within group decomposition. For each group g , decompose its total variance τ_g^2 into the variances of its coefficients. Denote the within-group proportions by $\varphi_g = (\varphi_{g1}, \dots, \varphi_{gp_g})$, with $\varphi_{gl} \geq 0$ and $\sum_{l=1}^{p_g} \varphi_{gl} = 1$. The variances of the individual coefficients b_{gl} are then given by

$$\text{Var}(b_{gl}) = \lambda_{gl}^2 \sigma^2 = \varphi_{gl} \tau_g^2 \sigma^2 = \varphi_{gl} \phi_g \tau^2 \sigma^2, \quad l = 1, \dots, p_g, \quad g = 1, \dots, G.$$

To complete the specification of the joint prior, we assume that R^2 follows a beta distribution with prior mean μ_{R^2} and precision ν_{R^2} . This facilitates an intuitive incorporation of domain knowledge into the R2 prior, as μ_{R^2} and ν_{R^2} can be directly communicated with users. From Equation 4, it follows that τ^2 is distributed according to a Beta Prime distribution with scales a_1, a_2 (Bai and Ghosh, 2021), where (a_1, a_2) denote the canonical parameters of the Beta distribution. Their relationship between the mean and precision is $\mu_{R^2} = a_1 / (a_1 + a_2)$ and $\nu_{R^2} = a_1 + a_2$. We will make use of both parametrizations in the paper.

Figure 1 illustrates the flexibility of Beta distributions in encoding prior beliefs about R^2 . It also shows the implied Beta Prime prior on τ^2 . When the parameters are set to

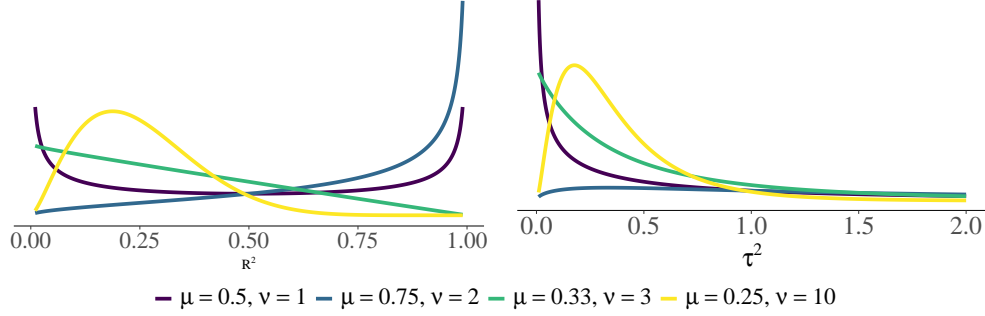


Figure 1: Beta and Beta Prime densities for several values of the prior mean μ_{R^2} and precision ν_{R^2} .

$(\mu_{R^2}, \nu_{R^2}) = (0.5, 1)$, the resulting prior on R^2 is bathtub-shaped, placing most of its mass near 0 and 1. This reflects a belief that the model is likely to explain either very little or nearly all of the variance—indicating an expectation of either predominantly noise or strong signal.

The proportions of group variance ϕ and within-group variance φ_g lie on the simplex. The canonical distribution for the simplex is the Dirichlet distribution, parameterized by the concentration vector α (Bhattacharya et al., 2015; Lin, 2016). This vector α fully determines the mean and correlation structure of the Dirichlet distribution. A parsimonious choice within this family is the symmetric Dirichlet distribution, where $\alpha = (a_\pi, \dots, a_\pi)$ with $a_\pi > 0$. We denote this distribution as $\phi \sim \text{Dirichlet } s(a_\pi)$, where $s(\cdot)$ emphasizes the symmetry of the concentration parameters. This choice greatly simplifies the number of hyperparameters to specify and facilitates the development of theoretical properties of the prior.

An alternative distribution for the simplex that has shown promise in R2 decomposition based settings is the logistic normal Aguilar and Bürkner (2025). This arises by mapping a multivariate normal distribution into the simplex via softmax transformations (Aitchison and Shen, 1980; Aitchison, 1986). Unlike the Dirichlet, the logistic normal allows for richer and more flexible dependency structures, as it can capture positive and negative correlations among components. In the following, we consider ϕ, φ_g to follow Dirichlet distributions as this simplifies studying the derivation of the prior’s mathematical properties.

To fully specify the joint hierarchical prior, we require a kernel for the coefficients b_{gl} . Consistent with the approaches of Aguilar and Bürkner (2023, 2025) and Kohns et al. (2025), we model b_{gl} as normally distributed with variance $\text{Var}(b_{gl}) = \sigma^2 \lambda_{gl}^2$.² The overall procedure to construct the Group-R2 prior is illustrated in Figure 2.1.

²An alternative is presented in Zhang et al. (2020), who use a Laplace kernel to induce strong marginal concentration of the coefficients around zero. However, Schmidt and Makalic (2020) show that the asymptotic properties of this choice are equivalent to those obtained using a normal kernel.

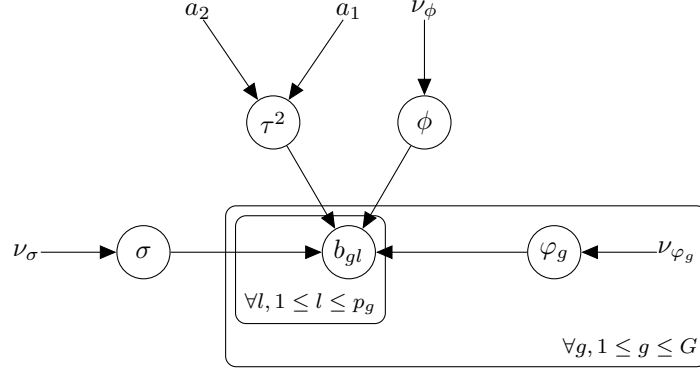


Figure 2: Directed acyclic graph (DAG) representing the prior structure of the Group-R2 decomposition prior. A global scale parameter τ^2 , governed by hyperparameters a_1 and a_2 , controls the total variance allocated across groups. The vector ϕ represents a group-level variance decomposition, drawn from a distribution over the simplex parameterized by ν_ϕ . For each group g , a within-group allocation vector φ_g is drawn from another simplex distribution with parameter ν_{φ_g} . Each coefficient b_{gl} inherits its prior variance through the product $\varphi_{gl}\phi_g\tau^2\sigma^2$. Plates indicate replication over groups ($g = 1, \dots, G$) and coefficients within groups ($l = 1, \dots, p_g$). This illustrates how variance is hierarchically allocated across and within groups.

We place a half Student- t prior on σ with η_σ degrees of freedom and scale parameter ν_σ , noting that both the prior mean and variance are proportional to ν_σ (Gelman, 2006; Goodrich et al., 2020). If a Gibbs sampler is preferred, an inverse gamma prior for σ^2 may be used as a computationally convenient alternative. The intercept b_0 is typically assigned either a normal prior or an improper uniform prior to ensure flexibility in modeling the overall mean.

The complete Group-R2 prior has the following form:

$$\begin{aligned} b_{gl} \mid \varphi_g, \phi, \tau^2, \sigma^2 &\sim \text{Normal}(0, \varphi_{gl}\phi_g\tau^2\sigma^2) \\ \phi &\sim \text{Dirichlet}(\cdot), \quad \varphi_g \sim \text{Dirichlet}(\cdot), \\ \tau^2 &\sim \text{BetaPrime}(\mu_{R^2}, \varphi_{R^2}), \quad \sigma \sim \pi(\sigma). \end{aligned} \tag{6}$$

2.2 Related priors

The Group Inverse-Gamma Gamma (GIGG) prior, introduced by Boss et al. (2023), is a recent advancement in the class of continuous shrinkage priors that explicitly account for known grouping structures among covariates. Like the Group-R2 prior, this prior is designed for regression settings with block-correlated regressors, where effective shrinkage must balance signal detection and variance control across and within groups.

The GIGG prior extends the global-local shrinkage framework by introducing a third, group-specific layer of hierarchy. Each coefficient b_{gl} is modeled as conditionally normal

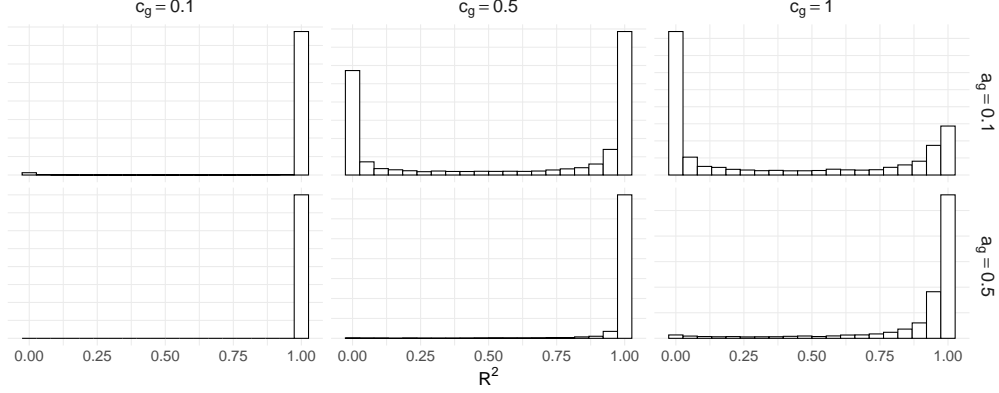
Implied Prior on R^2 with the GIGG Prior

Figure 3: Implied prior distributions on R^2 under the GIGG prior for various combinations of a_g, c_g . We obtain the distributions via Monte Carlo and consider $G = 10$ groups, $p = 50$ covariates and we have fixed $\sigma = 1$. The value a_g controls group-level shrinkage while c_g governs within-group shrinkage. The induced R^2 distribution varies substantially with these parameters, often lacking direct interpretability or control.

with variance proportional to the product $\tau^2 \gamma_g^2 \lambda_{gl}^2$, where τ^2 is a global scale, γ_g^2 is a group-specific scale, and λ_{gl}^2 is a local (coefficient-specific) scale. These scales are assigned the priors $\gamma_g^2 \sim \text{Gamma}(a_g, 1)$ and $\lambda_{gl}^2 \sim \text{Inv-Gamma}(c_g, 1)$, where we parameterize the gamma distribution in terms of shape and rate. This hierarchical structure induces a beta prime distribution on the product $\gamma_g^2 \lambda_{gl}^2$.

Boss et al. (2023) show that the hyperparameter a_g primarily governs the strength of thresholding, as it controls the spike at zero in the marginal distribution of b_{gl} . In contrast, c_g regulates the degree of shrinkage dependence within each group, influencing how strongly individual coefficients borrow strength from one another. This structure enables the GIGG prior to adaptively modulate shrinkage according to both the sparsity and correlation patterns present in the grouped design. Setting $c_g = a_g = 0.5$ is special, because it implies a group-horseshoe prior which collapses to the standard horseshoe prior of Carvalho et al. (2009), when the group-size is 1.

Figure 3 illustrates the implied prior distribution on R^2 under the GIGG prior across various settings of (a_g, c_g) . The results show that although the GIGG prior supports both group- and coefficient-level shrinkage, it does not offer explicit or intuitive control over the prior mass on R^2 . The shape and spread of the induced R^2 distributions vary considerably with hyperparameter choices and can lead to undesired concentration away from interpretable target regions (e.g., low or moderate R^2 values). In contrast, the Group- R^2 prior explicitly parameterizes R^2 , allowing users to encode prior beliefs about explained variance both at a global and group-level more directly and transparently.

While we were conducting this research, Yanchenko et al. (2025b) independently

proposed a related Group R^2 prior that also employs a hierarchical decomposition of explained variance across groups and within groups. The two developments were carried out in parallel and were motivated by related ideas in R^2 -based prior formulations.

2.3 Group-wise explained variances

In the following we introduce and characterize group-wise explained variances R_g^2 , which quantify the share of total explained variance attributable to each predictor group. This helps interpret how the Group R^2 prior distributes variance across groups, complementing the global R^2 perspective. We derive properties of R_g^2 and related quantities, such as the marginal distributions of group variances τ_g^2 and coefficient specific variances λ_{gl}^2 . These results will help us in our discussion on theory, shrinkage behavior, and hyperparameter specification shown thereafter.

Under the assumptions presented in Section 2.1, we define a group-specific explained variance metric R_g^2 as:

$$R_g^2 = \frac{\text{Var}(x'_g b_g)}{\text{Var}(x' b) + \sigma^2} = \frac{\tau_g^2}{\tau^2 + 1}, \quad g = 1, \dots, G. \quad (7)$$

Equivalently,

$$R_g^2 = \frac{\tau_g^2}{\tau^2 + 1} = \frac{\phi_g \tau^2}{\tau^2 + 1} = \phi_g R^2.$$

The quantity R_g^2 can be interpreted as the proportion of the total variance explained by the predictors in the g th group. Proposition 1 characterizes the joint distribution of R_g^2 and shows that $R_g^2, R_h^2, h \neq g$ will exhibit negative dependencies. Something we could expect since $\sum_{g=1}^G R_g^2 = R^2$. Proofs can be found in the Supplementary Results (Aguilar et al., 2025).

Proposition 1. (Joint distribution of R_g^2) If $\phi \sim \text{Dirichlet}(\alpha)$ then the following holds.

1. The joint distribution of $(R_1^2/R^2, \dots, R_G^2/R^2) = \phi \sim \text{Dirichlet}(\alpha)$.
2. $R_g^2/R^2 = \phi_g \sim \text{Beta}(\alpha_g, \sum_{j \neq g} \alpha_j)$.
3. The conditional distribution $(R_1^2, \dots, R_G^2) \mid R^2 = r^2 \sim r^2 \text{Dirichlet}(\alpha)$. Given $g \neq h$ then

$$\text{Cov}(R_g^2, R_h^2 \mid R^2 = r^2) = (r^2)^2 \text{Cov}(\phi_g, \phi_h) = -(r^2)^2 \frac{\alpha_g \alpha_h}{\alpha_0^2 (\alpha_0 + 1)},$$

$$\text{where } \alpha_0 = \sum_{i=1}^G \alpha_i.$$

When $\phi \sim \text{Dirichlet}(\alpha)$, the distribution of $R_g^2 = \phi_g R^2$ corresponds to the product of two Beta-distributed random variables. A closed-form expression exists, however it is typically too cumbersome to be useful in practice, so we do not present it here. Its

full derivation can be found in [Coelho and Alberto \(2021\)](#). However, the k th moment of R_g^2 can be found under a closed form and the set of them will completely determine its distribution ([Schmüdgen, 2020](#)):

$$\mathbb{E}[(R_g^2)^k] = \mathbb{E}[(\alpha_g)^k] \mathbb{E}[(R^2)^k] = \left(\prod_{i=0}^{k-1} \frac{\alpha_g + i}{\alpha_0 + i} \right) \left(\prod_{j=0}^{k-1} \frac{a_1 + i}{a_1 + a_2 + i} \right), \quad k \in \mathbb{N}. \quad (8)$$

For instance if $\phi_g \sim \text{Beta}(\alpha_g, 1)$ and $R^2 \sim \text{Beta}(\alpha_g + 1/2, 1)$ then we can conclude that $R_g^2 \sim \text{Beta}^2(2\phi_g, 1)$.

We characterize the marginal distributions of the total variance of the g th group τ_g^2 and the variances λ_{gl}^2 in Proposition 2. These results will be used in Section 2.4 to establish properties of our prior. Additionally, it will be useful for hyperparameter specification in Section 2.5.

Proposition 2. (*Marginals of τ_g^2 and λ_{gl}^2*) Let $a_G > 0$, $\tau^2 \sim \text{BetaPrime}(Ga_G, a_2)$, and $\phi \sim \text{Dirichlet } s(a_G)$, and $\varphi_g \sim \text{Dirichlet } s(c_g)$ with $c_g = a_G/p_g$ then:

1. The group-wise explained variance $\tau_g^2 = \phi_g \tau^2 \sim \text{BetaPrime}(a_G, a_2)$ marginally and independently.
2. The coefficient-specific variances $\lambda_{gl}^2 = \varphi_{gl} \tau_g^2$ are marginally distributed as $\lambda_{gl}^2 \sim \text{BetaPrime}(c_g, a_2)$.

Proposition 2 demonstrates that aligning the concentration parameters across the two decomposition levels yields a closed-form expression for the marginal distribution of the coefficient specific variances λ_{gl}^2 . Under this formulation, $c_g \leq a_G$, indicating that the within-group shrinkage will be stronger than the group-level shrinkage ([Aguilar and Bürkner, 2025](#)). Note that specifying the second-level concentration parameter c_g becomes immediate once the first-level parameter a_G is chosen. In other words, if we have an idea of the desired group-level shrinkage, the corresponding coefficient-level shrinkage follows directly. Conversely, if we instead have information about the within-group concentration parameters b_g , we can set $a_G = \frac{1}{G} \sum_{g=1}^G p_g c_g$, ensuring consistency with the assumptions of Proposition 2 while pooling information across groups to determine group-level shrinkage. For example if $a_G = 1$ and we have 10 covariates in a specific group, then $c_g = 0.1$. On the other hand if we have 5 groups with 10 coefficients each, and $c_g = 1$ then $a_G = 10$.

Proposition 3 characterizes the dependence structure induced by the Group-R2 prior on the marginal variance proportions $\phi_g \varphi_{gj}$. In particular, it quantifies both the covariance and correlation of their logarithms, $\log(\phi_g \varphi_{gj})$ and $\log(\phi_g \varphi_{gk})$, for $j \neq k$. These log-scale quantities have been highlighted by [Schmidt and Makalic \(2020\)](#) and [Tew et al. \(2025\)](#) as a useful mean to understand the concentration and tail behavior of shrinkage priors. This perspective becomes useful since we can apply the bilinear properties of the covariance operator. We extend the results of [Tew et al. \(2025\)](#) to the

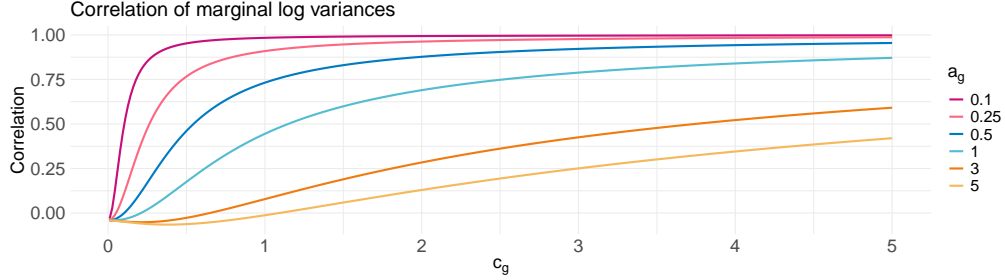


Figure 4: Correlation between marginal log-variances $\log(\phi_g \varphi_{gj})$ and $\log(\phi_g \varphi_{gk})$, $j \neq k$ within a group, as a function of the within-group concentration c_g , for different values of the group-level concentration a_g . Higher a_g leads to faster increases in correlation with respect to c_g , while low c_g can induce weak or even negative correlations

case in which dependencies are considered for the within-group scales, allowing us to capture richer covariance structures than priors with independent scales.

Proposition 3. (*Within-group variances dependency*) Assume that $a_G > 0$, $\tau^2 \sim \text{BetaPrime}(Ga_G, a_2)$, $\phi \sim \text{Dirichlet}(s(a_G))$, $\varphi_g \sim \text{Dirichlet}(s(c_g))$, ϕ and φ independent and consider the g th group. The following holds:

1. In general, $\text{Corr}(\log(\phi_g \varphi_{gj}), \log(\phi_g \varphi_{gk})) = \frac{\text{Var}(\log \phi_g) + \text{Cov}(\log \varphi_{gj}, \log \varphi_{gk})}{\text{Var}(\phi_g) + \text{Var}(\log \varphi_g)}$
2. Specifically for the assumptions considered we have that
 - $\text{Corr}(\log(\phi_g \varphi_{gj}), \log(\phi_g \varphi_{gk})) = \frac{\psi_1(a_g) - \psi_1(Ga_g) - \psi_1(p_g c_g)}{\psi_1(a_g) - \psi_1(Ga_g) + \psi_1(c_g) - \psi_1(p_g c_g)}$
 - $\text{Cov}(\phi_g \varphi_{gj}, \phi_g \varphi_{gk}) = \frac{a_g(a_g+1)}{(Ga_g)(Ga_g+1)} \frac{c_g}{p_g(c_g p_g + 1)} - \frac{1}{G^2 p_g^2}$

Our framework introduces structured dependencies among the variances assigned to coefficients by using Dirichlet priors for both ϕ and φ_g . The second decomposition stage, parameterized by c_g , plays a key role in modulating these within-group correlations. As shown in Figure 4, the correlation between $\log(\phi_g \varphi_{gj})$ and $\log(\phi_g \varphi_{gk})$ increases with c_g , with the speed of this increase controlled by the group-level parameter a_g . Notably, for small values of c_g , the correlation can be negative, a behavior that cannot arise under priors like GIGG or GRASP, where group-specific scales are modeled independently (Tew et al., 2025).

2.4 Marginal and joint distributions

In this section, we explore the marginal distribution of the coefficients b_{gl} and the joint distribution of the coefficients within a group when τ_g^2 is specified. We demonstrate that the marginal coefficients exhibit polynomial tails and high concentration near the

origin. Furthermore, we show that the joint distribution of the coefficients within each group displays a pronounced spike at zero. We also show that our prior can represent the horseshoe prior as a special case (Carvalho et al., 2010), hence expecting it to inherit the desirable properties from the latter.

For simplicity, we set $\sigma^2 = 1$ in the following derivations, although we clarify that all results are conditional on σ^2 , consistent with common practice in the analysis of marginal distributions in shrinkage priors (Bhattacharya et al., 2015; Pas, 2021; Bai and Ghosh, 2021). We denote the Beta and Gamma functions by $B(\cdot, \cdot)$ and $\Gamma(\cdot)$, respectively, and use $U(\eta, \nu, z)$ to represent the confluent hypergeometric function of the second kind (Jeffrey et al., 2007; Olver et al., 2010b). In the following we assume that $a_G > 0$, $R^2 \sim \text{Beta}(Ga_G, a_2)$, $\phi \sim \text{Dirichlet}(s(a_G))$, and $\varphi_g \sim \text{Dirichlet}(s(c_g))$ with $c_g = a_G/p_g$.

Proposition 4 (Marginal distributions of b_{gl}). *The marginal prior density of b_{gl} for any $g = 1, \dots, G$ and $l = 1, \dots, p_g$ is*

$$p(b_{gl}) = \frac{1}{\sqrt{2\pi} B(c_g, a_2)} \Gamma(\eta) U(\eta, \nu_g, z_{gl}), \quad (9)$$

where $\eta = a_2 + 1/2$, $\nu_g = 3/2 - c_g$, and $z_{gl} = |b_{gl}|^2/2$. Alternatively, if the within-group concentration parameters c_g are specified and a_G is set as $a_G = 1/G \sum_{g=1}^G p_g c_g$, the same conclusion follows.

Proposition 5 (Marginal distributions of b_{gl} near the origin). *As $|b_{gl}| \rightarrow 0$, with $0 < c_g \leq 1/2$ and $a_2 > 0$ the marginal prior densities are unbounded and exhibit a singularity at zero. Specifically, they satisfy*

$$p(b_{gl}) \sim \begin{cases} c_1 |b_{gl}|^{2c_g-1} + \mathcal{O}(|b_{gl}|^{2c_g+1}), & c_g < \frac{1}{2}, \\ -c_2 \ln(b_{gl}^2) + \mathcal{O}(b_{gl}^2 \ln(b_{gl}^2)), & c_g = \frac{1}{2}, \end{cases} \quad (10)$$

where $c_1, c_2 > 0$. Conversely, when $c_g > \frac{1}{2}$, the marginal prior densities are bounded and continuous at zero. Furthermore, they are differentiable at $b_{gl} = 0$ for all $c_g \geq 1$.

Proposition 5 shows that the interplay between the two levels of decomposition directly governs the behavior of the marginal priors near the origin, which in turn determines the amount of shrinkage imposed on the coefficients. Specifically, since the proposition requires $c_g \leq a_G$, it suggests that the within-group shrinkage is stronger than the group-level shrinkage. This ensures sufficient prior mass near zero, a crucial property for shrinkage priors to effectively detect and suppress irrelevant signals (Pas et al., 2014, 2017; Pas, 2021).

As c_g decreases from $1/2$ to zero, the prior shifts an increasing amount of mass toward the origin, resulting in posterior distributions that provide sparse estimates of the coefficient vector b . Conversely, when c_g exceeds $1/2$, the marginal priors become bounded at zero, favoring less sparse coefficient estimates. Thus, the parameter c_g offers a flexible mechanism for translating prior beliefs about sparsity (or the lack thereof) into the prior model, controlling the degree of shrinkage applied to the coefficients.

The tails of the prior play a crucial role in determining whether large signals can be detected and how strongly these signals are pulled back toward zero (Armagan et al., 2013; Pas et al., 2016; Pas, 2021). Ideally, priors with heavy tails are favored because they protect substantial signals from being overly shrunk (Carvalho et al., 2010; Piironen and Vehtari, 2017). This results in priors of bounded influence, meaning that truly large coefficients remain relatively unshrunk by the prior, i.e if $X = I$, then $\mathbb{E}[b_i | y_i] \approx y_i$ when y_i is greater than a threshold. This phenomenon, also known as tail robustness (Carvalho et al., 2010; Pas, 2021), is essential in sparse settings to selectively shrink only the smallest coefficients while leaving larger, genuine signals largely untouched. We show in Proposition 6 that the Group-R2 prior attains heavier tails than the Cauchy distribution and then establish in Proposition 7 that it can represent the horseshoe prior and is therefore of bounded influence.

Proposition 6 (Tails of the marginal prior). *As $|b_{gl}| \rightarrow \infty$, the marginal prior density of b_{gl} satisfies*

$$p(b_{gl}) \sim \mathcal{O}\left(\frac{1}{|b_{gl}|^{2a_2+1}}\right). \quad (11)$$

In particular, when $0 < a_2 \leq \frac{1}{2}$, the marginal priors have heavier tails than the Cauchy distribution.

Proposition 7 (Horseshoe type behavior). *If $c_g = a_2 = \frac{1}{2}$, then the marginal distributions of the Group-R2 prior are the same as the horseshoe prior, therefore the Group-R2 prior has bounded influence.*

We can find the joint distribution of the coefficients within a group by integrating over the group variance parameter $\tau_g^2 = \phi_g \tau^2$. This approach is similar to the idea presented by Boss et al. (2023), where integrating out variance parameters leads to conditional densities for grouped coefficients.

Proposition 8 (Joint distribution of group coefficients). *The joint distribution of the coefficients of the g th group, conditional on φ_g , is given by*

$$p(b_g | \varphi_g) = \frac{(2\pi)^{-p_g/2}}{B(c_g, b)} \left(\prod_{i=1}^{p_g} \varphi_{gi} \right)^{-1/2} \Gamma(\eta) U(\eta, \nu_g, z_g), \quad (12)$$

where $\eta = a_2 + \frac{p_g}{2}$, $\nu_g = 1 + \frac{p_g}{2} - c_g$, and $z_g = \sum_{l=1}^{p_g} \frac{b_{gl}^2}{\varphi_{gi}}$. Moreover, whenever $c_g < p_g/2$ and $b_{gl} \rightarrow 0$ for all $l = 1, \dots, p_g$, the joint density $p(b_g | \varphi_g)$ diverges to infinity.

The divergence of the joint density at zero for $c_g \leq 1/2$ indicates that the prior allocates substantial mass near zero, resulting in an infinite spike at the origin. This implies that we are able to shrink entire groups of coefficients if they are deemed as noise. Notably, when $p_g = 1$, the group consists of a single coefficient, and we recover the marginal prior distributions presented in Proposition 4. It is also worth noting that Equation 12 does not exhibit a traditional correlation structure, at least not one that is immediately apparent from its analytical form. To properly analyze the dependency structures implied by this joint prior, one should move beyond conventional multivariate dependency metrics and consider alternative representations, such as the implied copula.

2.5 Shrinkage properties

In this section, we examine how the prior influences shrinkage at both the coefficient and group levels. We first analyze the distribution of shrinkage factors κ_{gl} , which determine how much each coefficient is pulled toward zero under the normal means model. We then study the effective number of nonzero coefficients, m_{eff} , as a global measure of sparsity. These results show how hyperparameter choices translate into different regularization patterns.

Shrinkage Factors

As is common in the shrinkage literature, we can characterize the effect of the prior through the properties of the posterior distribution. In particular, analyzing the posterior mean and variance of each coefficient b_{gl} provides insight into how the prior induces shrinkage. Assume the normal means setting, where $X = I$ and $p = n$. Then the posterior distribution of b_{gl} given y_{gl} and its prior variance $\lambda_{gl}^2 = \varphi_{gl}^2 \phi_g^2 \tau_g^2 \sigma^2$ is:

$$b_{gl} \mid y_{gl}, \lambda_{gl}^2 \sim \text{Normal} \left(\frac{\lambda_{gl}^2}{1 + \lambda_{gl}^2} y_{gl}, \frac{\lambda_{gl}^2}{1 + \lambda_{gl}^2} \sigma^2 \right). \quad (13)$$

In this context, the maximum likelihood estimate (MLE) of b_{gl} is simply y_{gl} (Castillo and Vaart, 2012). The quantity $\kappa_{gl} = \frac{1}{1 + \lambda_{gl}^2} \in (0, 1)$ thus quantifies the degree of shrinkage imposed on the MLE. When the prior variance λ_{gl}^2 is large, little shrinkage is applied and $\kappa_{gl} \rightarrow 0$, whereas small prior variances lead to stronger shrinkage with $\kappa_{gl} \rightarrow 1$. The posterior mean of b_{gl} is directly related to κ_{gl} via

$$\mathbb{E}(b_{gl} \mid y_{gl}) = (1 - \mathbb{E}(\kappa_{gl} \mid y_{gl})) y_{gl}. \quad (14)$$

Hence, studying the distribution of κ_{gl} is key to understanding when the posterior of b_{gl} will be centered near zero or not. This connection makes κ_{gl} a useful diagnostic for assessing effective shrinkage, especially in hierarchical or group-structured priors (Castillo et al., 2015; Pas et al., 2014, 2016; Bai and Ghosh, 2019).

Let $\kappa_g = (\kappa_{g1}, \dots, \kappa_{gp_g})'$ denote the vector of shrinkage factors for the g th group. Assume $\sigma^2 = 1$ and $R^2 \sim \text{Beta}(a_G, a_2)$ such that $\tau_g^2 = \phi_g \tau^2 \sim \text{BetaPrime}(a_G, a_2)$. We use the parametrization $\lambda_{gl}^2 = \varphi_{gl} \tau_g^2$, with $\varphi_g = (\varphi_{g1}, \dots, \varphi_{gp_g})$ distributed as a symmetric Dirichlet with parameter c_g .

Note that the local scale of each coefficient is bounded above by the group scale, since $\varphi_{gl} \in (0, 1)$ and $\sum_{l=1}^{p_g} \varphi_{gl} = 1$ implies $\lambda_{gl}^2 \leq \tau_g^2$. As a consequence, even when τ_g^2 is moderately large, some λ_{gl}^2 may remain small due to the Dirichlet structure, leading to persistent shrinkage for certain coefficients. In particular, if τ_g^2 is small, all λ_{gl}^2 will be small, and the group will experience strong shrinkage uniformly across its elements.

Conditional on τ_g^2 , the joint prior of κ_g is

$$p(\kappa_g \mid \tau_g^2) = \frac{\Gamma(c_g p_g)}{\Gamma(c_g)} (\tau_g^2)^{-p_g c_g} \prod_{l=1}^{p_g} (1 - \kappa_{gl})^{c_g - 1} (\kappa_{gl})^{-(c_g + 1)}. \quad (15)$$

which can be found by change of variables with the following transformation $\lambda_{gl}^2 = \varphi_{gl} \tau_g^2 = \frac{1 - \kappa_{gl}}{\kappa_{gl}}$. Therefore, the domain of κ_g is restricted to

$$\mathcal{K} = \left\{ \kappa_g \in (0, 1)^{p_g} \mid \sum_{l=1}^{p_g} \frac{1 - \kappa_{gl}}{\kappa_{gl}} = \tau_g^2 \right\}. \quad (16)$$

Since marginally $\varphi_{gl} \sim \text{Beta}(c_g, (p_g - 1)c_g)$, it follows that

$$\mathbb{E}(\kappa_{gl}^m \mid \tau_g^2) = {}_2F_1(m, c_g, c_g p_g, -\tau_g^2), \quad m > 1, \quad (17)$$

where ${}_2F_1(\alpha, \beta, \gamma, z)$ denotes the Gauss hypergeometric function (Jeffrey et al., 2007). Although the joint density $p(\kappa_g \mid \tau_g^2)$ does not reveal the dependency structure among components of κ_g , the use of Equation (17) together with a Taylor expansion reveals that $\text{Cov}(\kappa_{gk}, \kappa_{gl}) < 0$ for $k \neq l$. See the Appendix for details. Thus, the negative dependence implied by the Dirichlet structure of φ_g is inherited by κ_g . This negative dependence among shrinkage factors introduces an implicit competition within each group, where we find that increasing flexibility for one coefficient tightens shrinkage on others.

Finally, marginalizing out τ_g^2 yields the unconditional joint prior for κ_g :

$$p(\kappa_g) = \frac{\Gamma(c_g p_g)}{\Gamma(c_g)} \text{B}(a_G - p_g c_g, a_2 + p_g c_g) \prod_{l=1}^{p_g} (1 - \kappa_{gl})^{c_g - 1} (\kappa_{gl})^{-(c_g + 1)}. \quad (18)$$

Focusing on a single shrinkage factor κ_{gl} , its marginal density is proportional to

$$p(\kappa_{gl}) \propto (1 - \kappa_{gl})^{c_g - 1} \kappa_{gl}^{-(c_g + 1)}. \quad (19)$$

Setting $c_g < 1$ causes the density to diverge both as $\kappa_{gl} \rightarrow 1$ and as $\kappa_{gl} \rightarrow 0$, concentrating prior mass at both extremes. In contrast, choosing $c_g > 1$ should allow for more uniform treatment of coefficients. This aligns with the results we showed in Section 2.4, which showed that $c_g \leq 1/2$ creates spikes in the marginal priors of the coefficients. When $c_g = 1/2$, the density of κ_{gl} has a bathtub shape, considering that b_{gl} can either be noise or signal with equal preference.

Effective number of non-zero coefficients

A global summary of the shrinkage induced by the prior is provided by the effective number of nonzero coefficients, m_{eff} , defined as (Piironen and Vehtari, 2017)

$$m_{\text{eff}} = \sum_{i=1}^p (1 - \kappa_i), \quad (20)$$

where κ_i denotes the shrinkage factor associated with the i th coefficient b_i , where by construction $m_{\text{eff}} \leq p$. This quantity captures how the combination of global and local scales, encoded through κ_i , reduces model complexity.

Visualizing the prior distribution of m_{eff} is a practical tool for understanding how the choice of hyperparameters controls shrinkage. If the user has prior knowledge or expectations about the number of relevant coefficients, they can simulate the distribution of m_{eff} under different hyperparameter settings and select the configuration that aligns with their prior beliefs (Piironen and Vehtari, 2017; Aguilar and Bürkner, 2025). This approach is particularly useful in high-dimensional applications, where direct specification of priors on individual coefficients may be unintuitive or impractical.

We can also define a group-wise effective number of nonzero coefficients as

$$m_{\text{eff},g} = \sum_{l=1}^{p_g} (1 - \kappa_{gl}), \quad (21)$$

so that the total effective number of nonzero coefficients decomposes as

$$m_{\text{eff}} = \sum_{g=1}^G m_{\text{eff},g}. \quad (22)$$

Under strong global shrinkage, we expect m_{eff} to concentrate near zero, while under weak global shrinkage, it may approach p . Similarly, for each group g , strong shrinkage at the group level (e.g., small values of τ_g^2) will result in $m_{\text{eff},g}$ concentrating near zero, indicating that most coefficients in the group are shrunk strongly toward zero. In contrast, when τ_g^2 is large, we expect $m_{\text{eff},g}$ to approach p_g , reflecting a weakly regularized group with more non-negligible coefficients. Figure 5 displays simulations from the prior distribution of the group-wise effective number of nonzero coefficients, $m_{\text{eff},g}$, under varying values of a_G and c_g . Recall that a_G is the parameter of the symmetric Dirichlet distribution used in the first-stage decomposition (across groups), while c_g controls the second-stage allocation of variance within each group.

The value of a_G controls the prior mean of R^2 . As a_G increases, the expected prior mean does so as well, from approximately 0.8 when $a_G = 0.1$ to around 0.99 when $a_G = 5$. Although a symmetric Dirichlet does not favor any particular group, when $a_G < 1$ the distribution concentrates near the corners of the simplex, allocating most variance to a few groups. In contrast, for $a_G \geq 1$, the distribution tends to allocate variance more evenly across groups.

Given a fixed a_G , the total variance assigned to a group is limited by the Dirichlet partition. This constraint is evident in Figure 5: when a_G is small, stronger shrinkage occurs within groups regardless of c_g . Moving on to second decomposition, where within-group sparsity is influenced by c_g , shows that small values of c_g promote sparsity regardless of the a_G values, while larger values of c_g shift the prior mass of $m_{\text{eff},g}$ toward less sparse configurations.

Finally, we distinguish two types of signal structure within each of the groups: concentrated and distributed signals. In concentrated settings, a small number of covariates explain most of the group-level assigned variance. In such cases, we recommend hyperparameter configurations that induce a prior for $m_{\text{eff},g}$ concentrated near low values such

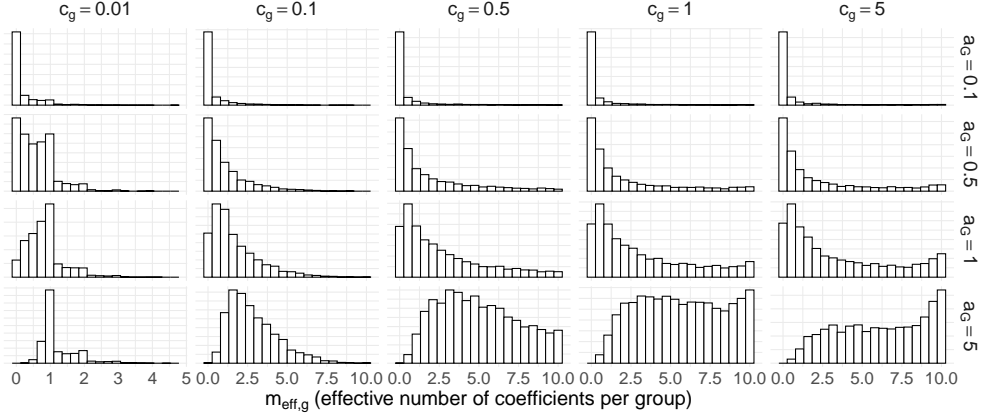


Figure 5: Prior predictive distributions of the group-wise effective number of nonzero coefficients ($m_{\text{eff},g}$) under different combinations of a_g, c_g for groups of size 10. Rows vary a_g , the concentration parameter of the group-level Dirichlet prior, and columns vary c_g , the within-group concentration.

as $a_g, c_g \leq 0.5$. Figure 5 shows that this settings shift mass towards low values of $m_{\text{eff},g}$. In distributed signal settings, where explanatory power is spread more evenly across group members, one may prefer priors where $m_{\text{eff},g}$ is centered near the half of the group size or has a broader distribution. Settings where $a_g \geq 0.5$ allow for this to happen as we show in Figure 5.

2.6 Hyperparameter specification

The Group R^2 prior introduces several hyperparameters that control shrinkage at different hierarchical levels: a_1, a_2 govern the prior on R^2 , while the concentration parameters of the Dirichlet distributions for ϕ and φ_g shape the variance decomposition across and within groups. These hyperparameters allow users to encode prior beliefs about model complexity, sparsity, and the expected contribution of each group of predictors. We recommend choosing them based on interpretability and the desired level of regularization.

The global scale of the prior is controlled via a Beta distribution on R^2 , denoted $R^2 \sim \text{Beta}(a_1, a_2)$, which induces a Beta prime distribution on the total variance τ^2 . The mean and concentration of this prior are given by $\mu_{R^2} = a_1/(a_1 + a_2)$ and $\nu_{R^2} = a_1 + a_2$, respectively. When prior information about R^2 is available from past studies or expert knowledge, the hyperparameters (μ_{R^2}, ν_{R^2}) can be set to reflect the mean and dispersion. For example, $a_1 = 1, a_2 = 1$ yields a uniform prior over R^2 . If $a_1 = a_2 = 0.5$, the resulting distribution on R^2 is bathtub like, expressing a belief that the model will either explain almost none or nearly all of the variance. This induces a bimodal shrinkage effect, discouraging intermediate levels of explained variance. Setting $a_2 = 0.5$ is a sensible

default, since the marginals of the coefficients will have Cauchy like tails, as shown in Section 2.4. The mean μ_{R^2} and precision ν_{R^2} can then be calibrated accordingly. This is the approach we follow in the simulations in Section 3.

The group-level allocation of variance is controlled by the Dirichlet prior $\varphi \sim \text{Dirichlet}(\cdot)$. A parsimonious choice is to consider a symmetric Dirichlet with parameter a_G , which governs the expected dispersion of variance across groups: values $a_G < 1$ favor sparsity by allocating most variance to a few groups, $a_G = 1$ yields a uniform prior, and $a_G > 1$ induces more even variance allocations. If little is known about the importance of different groups, setting $a_G = 1$ is a reasonable default (Lin, 2016; Aguilar and Bürkner, 2023). An alternative is to use the moments of R_g^2 presented in Equation 8 to communicate with users to specify the hyperparameters of R^2 and ϕ . Users are able to directly translate their beliefs about groups of coefficients into the prior by using the moments of R_g^2 .

Within each group, the proportion of variance attributed to individual coefficients is modeled using a second-level Dirichlet prior, $\phi_g \sim \text{Dirichlet}(\cdot)$. As in the first decomposition step, we suggest using a symmetric Dirichlet with parameter c_g that plays a similar role: small values ($c_g < 1$) promote sparsity within the group, while larger values yield more even allocations. We have exhibited this behavior in Figure 5. A particularly convenient choice stemmed from theory is $c_g = a_G/p_g$, which ensures that the marginal prior distribution of the coefficient variances λ_{gl}^2 has a closed-form Beta prime expression (see Proposition 4). This coupling allows the user to tune group-level shrinkage via a_G , while inducing coherent within-group behavior.

To guide hyperparameter selection, we recommend considering the anticipated sparsity structure. For scenarios where few groups are expected to matter and only a few coefficients per group are relevant, the combination $a_G < 1$ and $c_g < 1$ is appropriate. If group sizes are expected to be small but equally likely, $a_G = 1$ and $c_g = 1$ provides balanced shrinkage. Finally, the prior distribution of the effective number of coefficients m_{eff} or groupwise $m_{\text{eff},g}$ can be used to ensure that hyperparameter choices match prior expectations about model complexity, especially in high-dimensional settings.

Boss et al. (2023) propose using Marginal Maximum Likelihood Estimation (MMLE), an empirical Bayes approach, to automatically estimate hyperparameters. They implement MMLE iteratively within their Gibbs sampler for posterior inference. Even though MMLE offers an automatic procedure for specifying hyperparameters, this benefit is offset by the additional computational complexity it introduces, particularly when implemented within iterative sampling schemes. Moreover, our focus lies in understanding how the inclusion of prior information (especially through a small number of carefully chosen hyperparameters) is able to guide estimation and improve results, rather than relying on data-driven hyperparameter tuning.

3 Experiments

We have implemented the models with the probabilistic programming language and framework Stan (Carpenter et al., 2017; Stan Development Team, 2024), which employs

an adaptive Hamiltonian Monte Carlo (HMC) sampler known as the No-U-Turn Sampler (NUTS) (Neal, 2011; Brooks et al., 2011; Hoffman and Gelman, 2014) to sample draws from posterior distributions. The associated data and code are available at <https://github.com/jear2412/GroupR2priors>.

3.1 Evaluation Metrics

Our goal is to evaluate whether incorporating grouping structures into the prior improves the performance of R^2 decomposition priors, and under what conditions. To do so, we compare a baseline model M with its grouped counterpart M_G . For a given quantity of interest \mathcal{Q} , we define the performance difference as $\Delta\mathcal{Q} = \mathcal{Q}(M_G) - \mathcal{Q}(M)$. When the distribution of $\Delta\mathcal{Q}$ is centered around zero, both models perform similarly. The interpretation of $\Delta\mathcal{Q}$ depends on the specific quantity: higher values may indicate improvement or deterioration.

We evaluate four aspects of model performance: predictive performance, parameter recovery, coverage, and convergence. Results on predictive performance and parameter recovery are reported in the main text while coverage and convergence diagnostics appear in the Supplementary Material.

Out-of-sample Predictive Performance: We assess predictive performance using the expected log-pointwise predictive density (ELPD) (Vehtari and Ojanen, 2012; Vehtari et al., 2016), computed as

$$\text{ELPD} = \sum_{i=1}^{N_{\text{new}}} \ln \left(\frac{1}{S} \sum_{s=1}^S p(y_{\text{new},i} \mid \theta^{(s)}) \right),$$

where $\theta^{(s)}$ represents the s th draw from the posterior distribution $p(\theta \mid y)$ for $s = 1, \dots, S$. The ELPD quantifies predictive performance across a set of N_{new} observations unseen during model training. A value of $\Delta\text{ELPD} > 0$ indicates that the grouped version outperforms the nongrouped. To account for variation in the scale of ΔELPD across different models and simulation settings, we report asinh-transformed ΔELPD values in all figures. This transformation is given by $\text{asinh}(x) = \log(x + \sqrt{x^2 + 1})$ and behaves like a logarithm for large values while remaining linear around zero, facilitating interpretation of differences.

Parameter Recovery: We assess accuracy of parameter recovery by the posterior root mean squared error (RMSE) for each regression coefficient:

$$\text{RMSE} = \frac{1}{p} \sum_{i=1}^p \sqrt{\frac{1}{S} \sum_{s=1}^S (b_i^{(s)} - b_i)^2},$$

where $b_k^{(s)}$ is the s th posterior draw for coefficient b_k , and b_k is the true value. This global metric captures both systematic bias and estimation variance (Robert, 2007). To refine this assessment, we also report three types of RMSE: 1) across all coefficients, 2) for true zeros (evaluating shrinkage of irrelevant predictors), and 3) for true nonzeros (measuring

signal recovery). Lower RMSE values indicate better recovery; thus, $\Delta\text{RMSE} < 0$ favors the grouped model. We highlight that this is not the typical RMSE based in the posterior mean, but we are using the whole posterior distribution to calculate it.

Coverage: We assess 95% marginal credible interval coverage by reporting average coverage rates, interval widths, sensitivity, specificity (power), and nonzero coverage (Benjamini and Hochberg, 1995). We also examine how these metrics vary with interval width via Receiver Operating Characteristic (ROC) curves.

Convergence Diagnostics: We monitor the quality of posterior samples using two convergence indicators: 1) The potential scale reduction factor \hat{R} (Vehtari et al., 2021), which should be close to 1 if chains are well mixed. 2) The effective sample size (ESS), reflecting the effect of dependency compared to a sample of independent draws. High ESS values signal efficient sampling and low autocorrelation (Brooks et al., 2011).

3.2 Simulations

Data generating procedure

We base our simulation design on a modified version of the setup proposed by Boss et al. (2023). The design matrix X is drawn from a multivariate normal distribution with zero mean and covariance matrix Σ_X . The structure of Σ_X reflects a block-diagonal, exchangeable correlation pattern: variables within the same group have pairwise correlation $\rho_{\text{in}} = 0.8$, while variables across groups have $\rho_{\text{out}} = 0.2$. All covariates are standardized to have unit variance. The error variance σ^2 is set to achieve a prespecified $R^2 \in \{0.25, 0.80\}$. We fix the sample size to $n = 200$ for all experiments. Each group contains $p_g = 10$ covariates, so the total number of groups is $G = p/10$, with $p \in \{100, 500\}$.

We evaluate five scenarios for generating the regression coefficients b , each reflecting different assumptions about sparsity and signal distribution within groups. 1) **Concentrated:** The signal is sparse and localized within each group. The first coefficient of each group is nonzero and set to $b_{g1} = 2$ while all others are zero. 2) **Random concentrated:** A random variant of the previous one in which the first coefficient in each group is sampled independently from $\mathcal{N}(0, 3^2)$, with all other coefficients in the group set to zero. 3) **Distributed:** The signal is spread across the multiple covariates that belong to a group. In the deterministic version, only the first group is active, leading to the first 10 coefficients being nonzero. We set $b_i = 0.5$ for $i = 1, \dots, 5$ and $b_i = 1$ for $i = 6, \dots, 10$. 4) **Random distributed:** Similar to the distributed, but the first 10 coefficients of the active group are independently drawn from $\mathcal{N}(0, 3^2)$. In both cases, the remaining coefficients are set to zero. 5) **Random Coefficients:** Following Boss et al. (2023), the first group is randomly assigned either a concentrated or distributed signal with equal probability, ensuring the presence of at least one active group. For each of the remaining groups, a concentrated signal is assigned with probability 0.2, a distributed signal with probability 0.2, and no signal with probability 0.6.

Models

The grouped and nongrouped versions differ only in their hierarchical structure: the grouped models include the ϕ and φ_g decompositions, while the nongrouped ones do not. For Group-R2 priors, we specify symmetric Dirichlet distributions for both ϕ and φ_g , with $a_G \in \{0.1, 0.5, 1\}$ and $c_g = 0.5$, respectively. For the nongrouped (standard) R2D2 model, we also use a symmetric Dirichlet with $a_\pi = a_G$.

We adopt the marginal formulations developed in Section 2.4 in Propositions 5 and 6 to set the hyperparameters of the R^2 prior. Specifically, we let $a_1 = Ga_G$, where G is the number of groups, and fix $a_2 = 0.5$ to induce heavy tails and facilitate signal detection. This approach enables an automatic and principled specification of the R^2 prior in line with the theoretical results. The value $c_g = 0.5$ was chosen based on the expected effective number of nonzero coefficients m_{eff} . As discussed in Section 2.5, it allows for a variety of shapes for its distribution, enforcing sparsity when a_G is small and a uniform like behavior that spreads signal across group elements when a_G increases. A priori, this behaviors should accomodate for the different mechanisms by which we generate the coefficients. Since these models are fully characterized by the choice of a_G , we denote them as **R2- a_G** in the results.

We also evaluate two additional prior configurations and their grouped counterparts: 1) Uniform R2 prior **R2-u**: This baseline sets $a_1 = a_2 = 1$ for the R^2 prior, and uses symmetric Dirichlet distributions with $a_G = c_g = 1$ for the grouped version, or $a_\pi = 1$ for the nongrouped. This corresponds to uniform priors over both the total R^2 and the simplex partitions. 2) Concentrated and Distributed R2 Priors: These models share the same prior mean and variance for R^2 , with $(\mu_{R^2}, \nu_{R^2}) = (1/3, 3)$. They differ in how signal sparsity is structured. The concentrated version **R2-c** sets $a_G = 1$ and $c_g = 0.5$, promoting sparsity within each group. This setup should be better suited for concentrated signals, where only a few predictors per group are truly active. In contrast, the distributed version **R2-d** uses $a_G = 0.5$ and $c_g = 1$, placing more uniform prior mass across coefficients within a group and thereby supporting distributed signals, where multiple predictors share the signal. These configurations allow us to test whether tuning the decomposition hyperparameters to match the underlying sparsity pattern improves model performance.

Results

Lower-dimensional results We first evaluate the performance of Group-R2 priors in the lower-dimensional setting ($p = 100$, $n = 200$). Figure 6 reports the difference in out-of-sample predictive performance ΔELPD , while Figure 7 reports the difference in parameter recovery ΔRMSE . Overall, grouping improves predictive performance in scenarios where signal is distributed across covariates or randomly assigned (Distributed, Random Distributed, Random Coefficients), particularly when $R^2 = 0.8$. Gains in predictive performance tend to increase with the group-level concentration parameter a_G , as seen in the progression from models R2-0.1 to R2-1.0. In contrast, when signals are highly concentrated within groups (Concentrated), grouping provides little to no benefit in predictive performance. Moreover, fixing our attention in the concentrated and

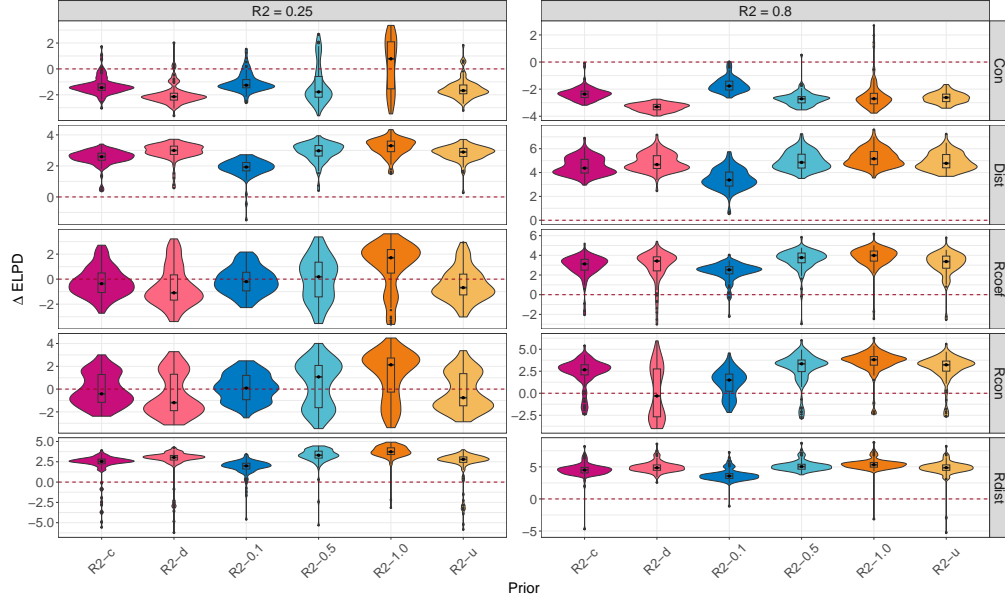


Figure 6: ΔELPD (asinh-transformed) for the lower-dimensional scenario ($p = 100, n = 200$). Values above the line indicate improvement in predictive performance when considering groups. “Con” denotes the concentrated signal, “Dist” the distributed signal, “Rcon” and “Rdist” their random counterparts, and “Rcoef” the random coefficients setting. Group-R2 priors improve predictive performance in distributed and mixed signal settings. Gains increase with a_G , especially when R^2 is high.

distributed rows, we observe a trade-off in prior assumptions: priors assuming distributed signals such as R2-d perform worse in the concentrated scenario than priors assuming concentrated scenario like R2-c.

Figure 7 shows that parameter recovery is consistently improved when grouping is taken into account, especially when R^2 is high. Once again, concentrated signals represent the most challenging scenario, where non-grouped models can sometimes match or outperform grouped ones. As with predictive performance, RMSE improves monotonically with increasing a_G in the Group-R2 priors. The uniform prior R2-u, which does not favor any particular sparsity structure, emerges as a robust default. It delivers competitive performance across different signal patterns when no prior knowledge about sparsity is available. The improvement in the cases in which the grouped priors outperform, as can be seen from Figure 8 and 9, come from improved shrinkage on the truly zero coefficients groups. This holds for true for low and high R^2 . Relatively weak performance of the grouped priors in the concentrated case comes from the fact that the truly non-zero coefficients in each group are over-shrunk, as indicated by higher ΔRMSE seen in the first row of Figure 9. Taken together, these results echo findings

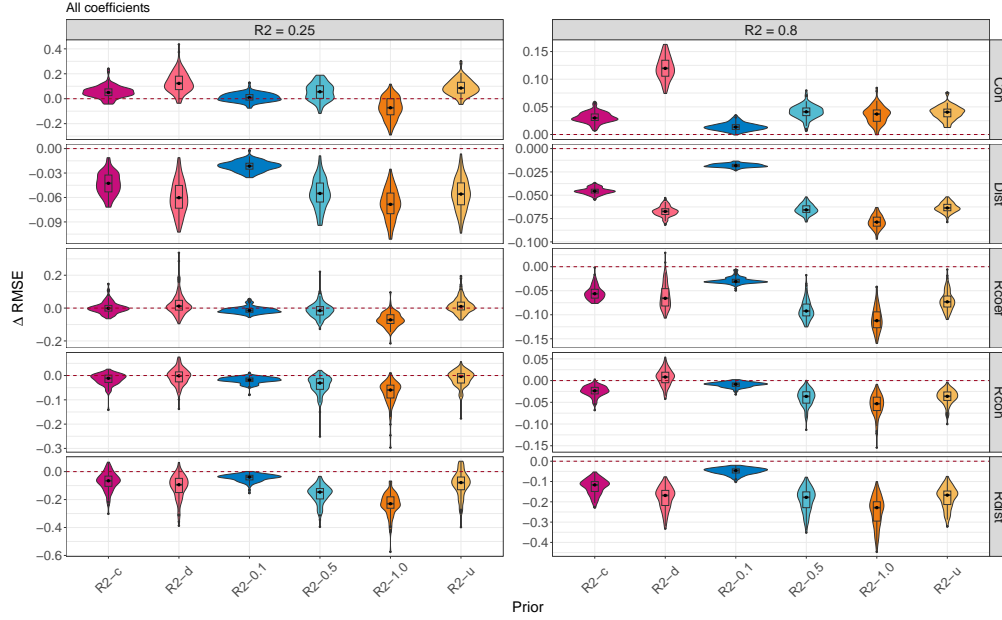


Figure 7: $\Delta RMSE$ for the lower-dimensional scenario ($p = 100$, $n = 200$). Values below the line indicate improvement in parameter recovery when considering groups. “Con” denotes the concentrated signal, “Dist” the distributed signal, “Rcon” and “Rdist” their random counterparts, and “Rcoef” the random coefficients setting. Group- R^2 priors consistently improve parameter recovery in distributed and mixed signal settings. Improvements grow with a_G ; the uniform prior performs robustly across different scenarios.

found in the group-prior literature such as [Boss et al. \(2023\)](#), in which the benefit to using group-priors comes from imposing correlation in shrinkage for groups of covariates for which the signal is weak.

High-dimensional results We now consider the high-dimensional setting with $p = 500$ and $n = 200$. Figures 10 and 11 show $\Delta ELPD$ and $\Delta RMSE$, respectively³.

The interpretation of the results remain the same. The results show similar patterns to the lower-dimensional case, but the benefits of incorporating group structure are amplified in high dimensions. In distributed signal settings, grouping leads to large gains in both predictive performance and parameter recovery, particularly when $R^2 = 0.8$. For the Random Coefficients case, improvement only comes when considering sufficiently high values for $a_G = 1$ and under high R^2 . Concentrated signals are still challenging.

³Break down of the $\Delta RMSE$ in terms of true zero and true non-zero are relegated to the Supplementary Material due to similarity to the lower-dimensional DGP results.

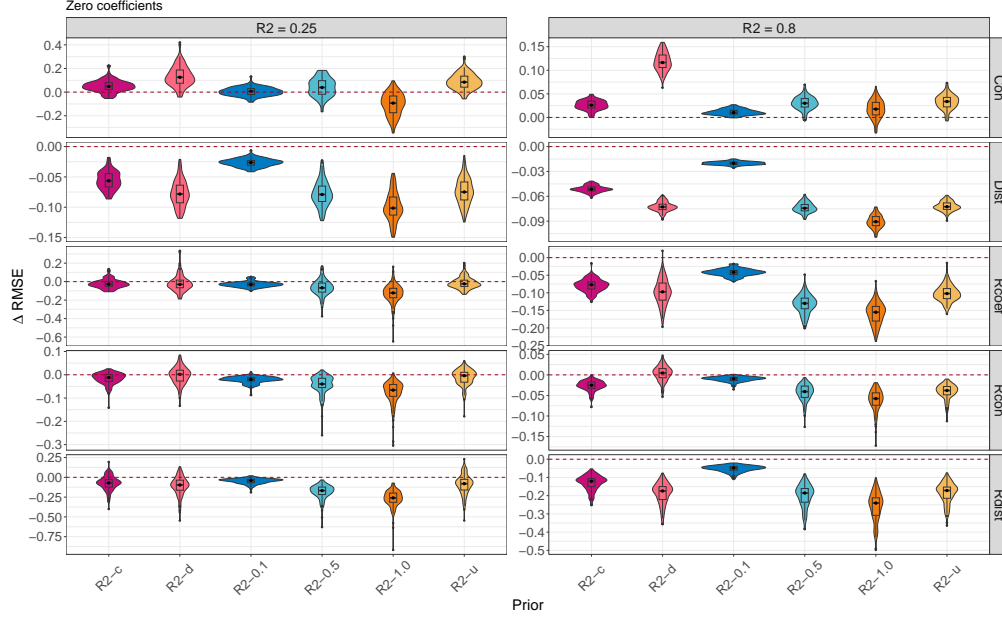


Figure 8: ΔRMSE for truly zero coefficients for the lower-dimensional scenario ($p = 100$, $n = 200$). Values below the line indicate improvement in parameter recovery when considering groups. “Con” denotes the concentrated signal, “Dist” the distributed signal, “Rcon” and “Rdist” their random counterparts, and “Rcoef” the random coefficients setting.

Inclusion of grouping structures does not outperform the baseline.

Figure 11 shows that the Group- R^2 priors consistently improve RMSE across distributed signal settings in the high-dimensional case. In contrast, no improvement is achieved under the Random Coefficients case. However performance does improve in this scenario as R^2 increases. Even though improvement is not strong in this case, including grouping structures in the prior is not detrimental either, as the distributions of ΔELPD are centered around zero. Concentrated signals are again challenging, however the loss involved by including groups is small.

4 Discussion

In this work, we introduced the Group- R^2 prior, analyzed its mathematical properties, and evaluated its empirical performance through simulations. The Group- R^2 prior is a modification of the R^2 shrinkage priors that incorporates known grouping structures through a two-stage hierarchical decomposition of the prior coefficient of determination R^2 . We first distribute the total variance across groups and then within each group

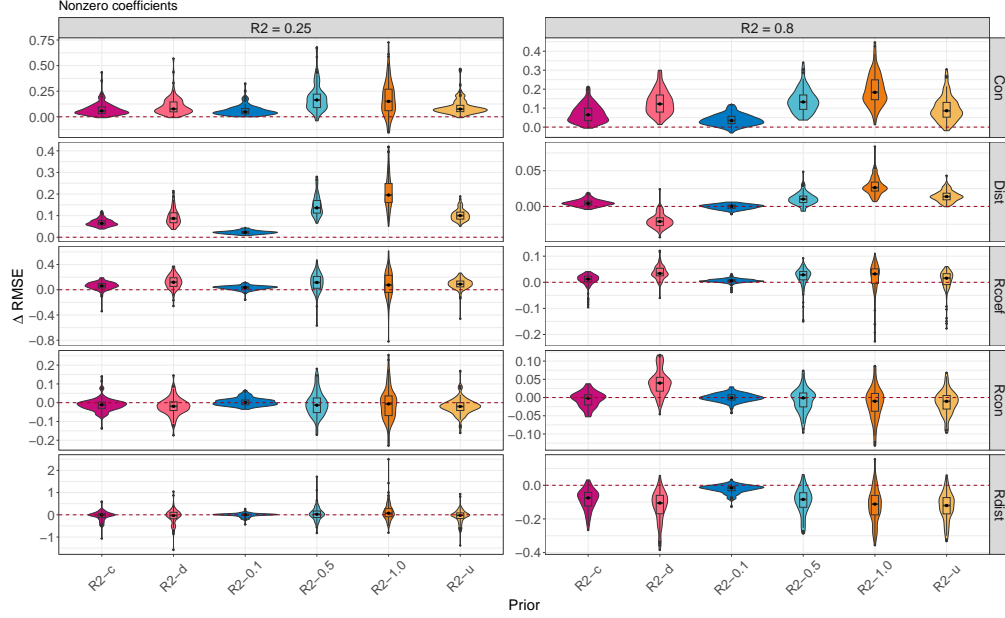


Figure 9: $\Delta RMSE$ for truly nonzero coefficients for the lower-dimensional scenario ($p = 100$, $n = 200$). Values below the line indicate improvement in parameter recovery when considering groups. “Con” denotes the concentrated signal, “Dist” the distributed signal, “Rcon” and “Rdist” their random counterparts, and “Rcoef” the random coefficients setting.

across individual coefficients. We have shown that this construction preserves desirable shrinkage properties—such as heavy tails and strong concentration near the origin, both at a marginal and group level. We have also shown how the choice of hyperparameters of the decomposition govern shrinkage behavior at both levels of the hierarchy. We have also provided a practical framework for hyperparameter calibration using interpretable diagnostics such as the effective number of non-zero coefficients.

Our simulation experiments complement our theoretical results and illustrate the practical value of incorporating grouping structures into R2-based priors. In both lower- and high-dimensional settings, Group R2 priors consistently improve parameter recovery when the signal is distributed across predictors or randomly mixed. In these scenarios, increasing a_G enhances recovery by encouraging more even allocations of variance across groups. Gains in predictive accuracy follow similar trends, especially in high dimensions. In contrast, when signals are highly concentrated within individual groups, the benefits of grouping are more modest and depend more on how well the prior matches the data generating process.

A key limitation of the current framework is its reliance on pre-specified group

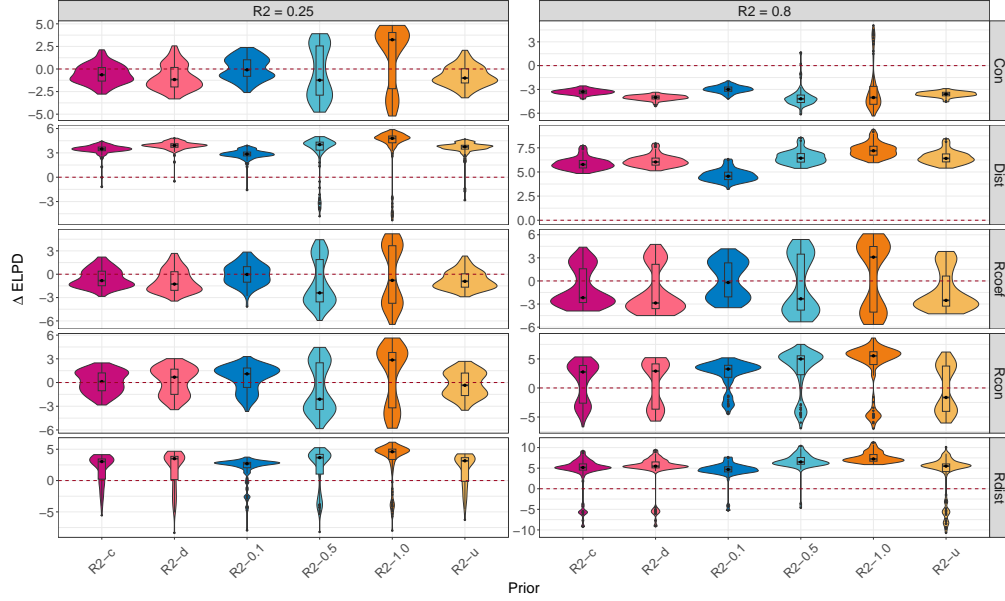


Figure 10: ΔELPD (asinh-transformed) for the high-dimensional scenario ($p = 500$, $n = 200$). Values above the line indicate improvement in predictive performance when considering groups. “Con” denotes the concentrated signal, “Dist” the distributed signal, “Rcon” and “Rdist” their random counterparts, and “Rcoef” the random coefficients setting. Group-R2 priors improve predictive performance in distributed signal settings. Performance in Random Coefficients (Rcoef) is mixed, with limited gains except when a_G is sufficiently high and high R^2 is present. Concentrated signals remain challenging.

structures, which are assumed to be known and fixed in advance. In practice, groups may be misspecified due to noisy prior knowledge or arbitrary definitions, leading to misallocation of variance and suboptimal shrinkage. For example, assigning signal covariates to low-variance groups can suppress important effects, while allocating variance to purely noisy groups may inflate uncertainty. This makes the method vulnerable to structural assumptions, particularly in settings where group definitions are uncertain or high-dimensional. Future work should focus on extending the Group R2 framework to settings where group structure is unknown or partially observed, for instance by coupling with latent group discovery methods or using external similarity measures to inform grouping.

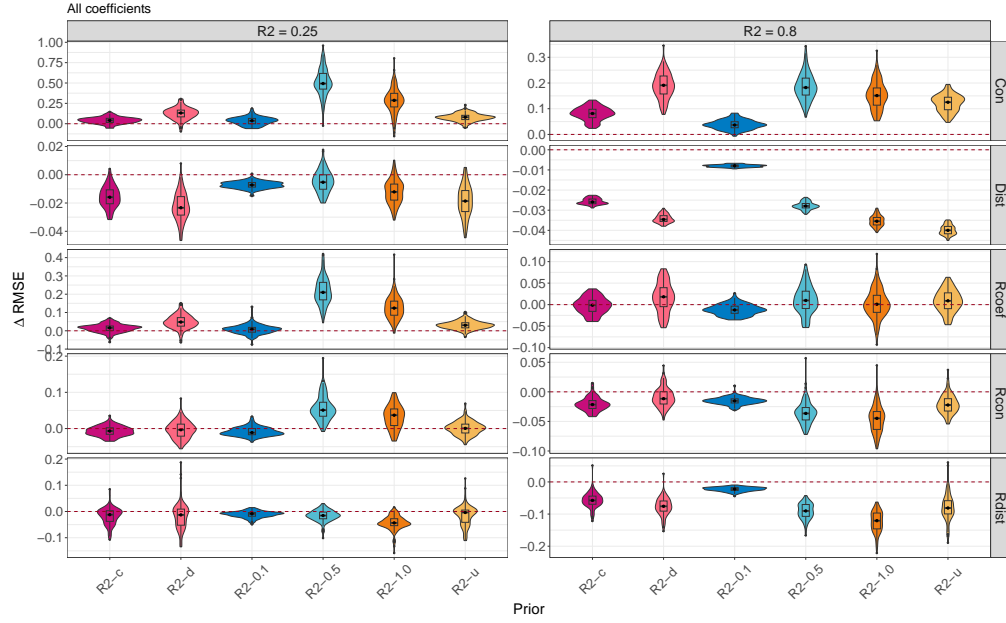


Figure 11: ΔRMSE for the high-dimensional scenario ($p = 500$, $n = 200$). Values below the line indicate improvement in parameter recovery when considering groups. “Con” denotes the concentrated signal, “Dist” the distributed signal, “Rcon” and “Rdist” their random counterparts, and “Rcoef” the random coefficients setting. Group-R2 priors improve parameter recovery across distributed and random signal settings, especially as a_G increases. In the concentrated case, no substantial improvement or deterioration is observed.

Acknowledgments

Funded by Deutsche Forschungsgemeinschaft (DFG, German Research Foundation) Project 500663361. Javier Enrique Aguilar and Paul-Christian Bürkner acknowledge the computing time provided on the Linux HPC cluster at Technical University Dortmund (LiDO3), partially funded in the course of the Large-Scale Equipment Initiative by DFG Project 271512359. Paul-Christian Bürkner further acknowledges support of the Deutsche Forschungsgemeinschaft (DFG, German Research Foundation) via the Collaborative Research Center 391 (Spatio-Temporal Statistics for the Transition of Energy and Transport) – 520388526. Javier Enrique Aguilar further acknowledges travel support from the European Union’s Horizon 2020 research and innovation programme under grant agreement No 951847. Javier Aguilar also acknowledges the support of F.c. and F.L for their contribution to the elaboration of this manuscript. David Kohns acknowledges the computational resources provided by the Aalto Science-IT project, and the support of the Research Council of Finland Flagship programme: Finnish Center for Artificial Intelligence, Research Council of Finland project (340721), and the Finnish Foundation for Technology Promotion.

5 Supplementary Results

5.1 Proofs

Proof of proposition 1

The proof follows by applying standard properties of the Dirichlet distribution. See [Lin \(2016\)](#) for details. \square

Proof of proposition 2

To prove the proposition we will use the following auxiliary propositions. Their proofs can be found in [Zhang et al. \(2020\)](#).

Proposition 9. *If $\tau^2 \mid \xi \sim Ga(a_1, \xi)$ and $\xi \sim Ga(a_2, 1)$, then $\tau^2 \sim \text{BetaPrime}(a_1, a_2)$.*

Proposition 10. *If $\tau^2 \mid \xi \sim Ga(a_1, \xi)$, $\phi \sim \text{Dirichlet}(s(a_\pi))$ of dimension k and $a_1 = ka_\pi$, then $\phi_j \tau^2 \mid \xi \sim Ga(a_\pi, \xi)$, $j = 1, \dots, k$ independently.*

1. By hypothesis we have that $\tau^2 \sim \text{BetaPrime}(Ga_G, a_2)$. Applying Proposition 9 yields

$$\tau^2 \mid \xi \sim Ga(Ga_G, \xi), \xi \sim Ga(a_2, 1).$$

Using Proposition 10 with $a_1 = Ga_G$ shows that $\tau_g^2 \mid \xi \sim \text{BetaPrime}(a_G, \xi)$. Therefore we have

$$\tau_g^2 \mid \xi \sim Ga(a_G, \xi), \xi \sim Ga(a_2, 1).$$

Applying Proposition 9 again gives $\tau_g^2 \sim \text{BetaPrime}(a_G, a_2)$. \square

2. The result follows by applying the same procedure that we have used to show the previous result but at a group level. \square

Proof of proposition 3

1. We are interested in the quantity

$$\text{Corr}(\log(\phi_g \varphi_{gj}), \log(\phi_g \varphi_{gk})) = \frac{\text{Cov}(\log(\phi_g \varphi_{gj}), \log(\phi_g \varphi_{gk}))}{\sqrt{\text{Var}(\log(\phi_g \varphi_{gj})) \text{Var}(\log(\phi_g \varphi_{gk}))}}, \quad j \neq k \quad (23)$$

Applying properties of the covariance operator and using the fact that ϕ_g and φ_g are independent we find that:

$$\text{Cov}(\log(\phi_g \varphi_{gj}), \log(\phi_g \varphi_{gk})) = \text{Cov}(\log(\phi_g) + \log(\varphi_{gj}), \log(\phi_g) + \log(\varphi_{gk}))$$

$$= \text{Var}(\log \phi_g) + \text{Cov}(\log \varphi_{gj}, \log \varphi_{gk}).$$

The main quantity in the denominator is $\text{Var}(\log(\phi_g \varphi_{gj}))$, which can be written as

$$\begin{aligned} \text{Var}(\log(\phi_g \varphi_{gj})) &= \text{Var}(\log(\phi_g) + \log(\varphi_{gj})) \\ &= \text{Var}(\log(\phi_g)) + \text{Var}(\log(\varphi_{gj})). \end{aligned}$$

Since $\varphi_g \sim \text{Dirichlet}(s(c_g))$, both φ_{gj} and φ_{gk} have the same marginal distributions and we have $\text{Var}(\log(\phi_g \varphi_{gj})) = \text{Var}(\log(\phi_g)) + \text{Var}(\log(\varphi_{g\cdot}))$. Therefore

$$\text{Corr}(\log(\phi_g \varphi_{gj}), \log(\phi_g \varphi_{gk})) = \frac{\text{Var}(\log \phi_g) + \text{Cov}(\log \varphi_{gj}, \log \varphi_{gk})}{\text{Var}(\log(\phi_g)) + \text{Var}(\log(\varphi_{g\cdot}))}. \quad \square \quad (24)$$

The result can be generalized to the case in which the proportions of explained variance do not follow a symmetric Dirichlet, but we do not show that here.

2. The result follows by substituting the following quantities in Equation (24):

$$\begin{aligned} \text{Var}(\log \phi_g) &= \psi_1(a_g) - \psi_1(Ga_g) \\ \text{Var}(\log \varphi_{gl}) &= \psi_1(c_g) - \psi_1(p_g c_g), \quad l \in \{1, \dots, p_g\} \\ \text{Cov}(\log \varphi_{gj}, \log \varphi_{gk}) &= -\psi_1(p_g c_g), \quad j \neq k \end{aligned}$$

where ψ_1 is the trigamma function (Olver et al., 2010b). \square

3. We have

$$\text{Cov}(\phi_g \varphi_{gj}, \phi_g \varphi_{gk}) = \mathbb{E}[\phi_g^2 \varphi_{gj} \varphi_{gk}] - \mathbb{E}[\phi_g \varphi_{gj}] \mathbb{E}[\phi_g \varphi_{gk}] \quad (25)$$

$$= \mathbb{E}[\phi_g^2] \cdot \mathbb{E}[\varphi_{gj} \varphi_{gk}] - \mathbb{E}[\phi_g]^2 \mathbb{E}[\varphi_{gj}] \mathbb{E}[\varphi_{gk}], \quad j \neq k. \quad (26)$$

where we have used the independence of ϕ_g, φ_g to expand the expectations. The expressions in the last line have closed analytical forms given by:

$$\begin{aligned} \mathbb{E}[\phi_g] &= \frac{1}{G}, \quad \mathbb{E}[\varphi_{gl}] = \frac{1}{p_g}, \quad l \in \{1, \dots, p_g\}, \\ \mathbb{E}[\phi_g^2] &= \frac{a_g(a_g + 1)}{(Ga_g)(Ga_g + 1)} \quad \mathbb{E}[\varphi_{gj} \varphi_{gk}] = \frac{c_g^2}{p_g^2(c_g p_g + 1)}, \quad j \neq k \end{aligned}$$

The result follows by substituting the expressions in Equation (25). \square

Proof of proposition 4

Under the assumptions considered, the Group-R2 prior has the following alternative representation

$$b_{gl} \mid \lambda_{gl}^2 \sim \text{Normal}(0, \lambda_{gl}^2) \quad \lambda_{gl}^2 \sim \text{BetaPrime}(c_g, a_2).$$

The prior marginal density of b_i is given by

$$\begin{aligned} p(b_{gl}) &= \int_0^\infty \frac{1}{\sqrt{2\pi\lambda_{gl}^2}} \exp\left\{-\frac{b_{gl}^2}{2\lambda_{gl}^2}\right\} \frac{1}{B(c_g, a_2)} (\lambda_{gl}^2)^{c_g-1} (\lambda_{gl}^2 + 1)^{-c_g-a_2} d\lambda_{gl}^2 \\ &= \frac{1}{\sqrt{2\pi} B(c_g, a_2)} \int_0^\infty \exp\left\{-\frac{b_{gl}^2}{2} t_{gl}\right\} t_{gl}^{\eta-1} (t_{gl} + 1)^{\nu-\eta-1} dt_{gl} \\ &= \frac{1}{\sqrt{2\pi} B(c_g, a_2)} \Gamma(\eta) U(\eta, \nu, z_{gl}), \end{aligned}$$

where $t_{gl} = \frac{1}{\lambda_{gl}^2}$, $\eta = a_2 + 1/2$ and $\nu = 3/2 - c_g$. $U(\eta, \nu, z_{gl})$ represents the confluent hypergeometric function of the second kind ([Jeffrey et al., 2007](#)) and $z_{gl} = \frac{|b_{gl}|^2}{2}$. The function $U(\eta, \nu, z_{gl})$ is defined as long as the real part of η and z_{gl} are positive, which is always the case since $a_2 > 0$ and $|b_{gl}| > 0$. \square

Proof of proposition 5

In the following we drop the index of z_{gl} , since all cases are handled equally. The confluent hypergeometric function of the second kind $U(\eta, \nu, z)$ satisfies the following identity [Olver et al. \(2010a\)](#).

$$U(\eta, \nu, z) = z^{1-\nu} U(\eta - \nu + 1, 2 - \nu, z). \quad (27)$$

Substituting $\eta = a_2 + 1/2$, $\nu = 3/2 - c_g$ and $z = \frac{t^2}{2}$ results in

$$U\left(a_2 + 1/2, 3/2 - c_g, \frac{t^2}{2}\right) = t^{2c_g-1} U\left(a_2 + c_g, c_g + 1/2, \frac{t^2}{2}\right).$$

The right hand side has a singularity at $t = 0$ when $c_g < 1/2$. We consider the limiting form U has as $|z| \rightarrow 0$ to study the order of concentration near the origin for different values of c_g . Equation 13.2.18 in [Olver et al. \(2010a\)](#) states

$$U(\eta, \nu, z) = \frac{\Gamma(\nu-1)}{\Gamma(\eta)} z^{1-\nu} + \frac{\Gamma(1-\nu)}{\Gamma(\eta-\nu+1)} + \mathcal{O}(z^{2-\nu}), \quad 1 < \nu < 2.$$

Substituting $\eta = a_2 + 1/2, \nu = 3/2 - c_g$ and $z = \frac{t^2}{2}$ results in

$$U\left(a_2 + 1/2, 3/2 - c_g, \frac{t^2}{2}\right) = Ct^{2c_g-1} + \frac{\Gamma(c_g + 1/2)}{\Gamma(a_2 + 1/2)} + \mathcal{O}(|t|^{1+2c_g}), \quad 0 < c_g < 1/2,$$

where $C = 2^{1/2-c_g} \frac{\Gamma(1/2-c_g)}{\Gamma(a_2+1/2)}$. The last expression is unbounded at $t = 0$ when $c_g < 1/2$. The case when $c_g = 1/2$ follows equation 13.2.19 in [Olver et al. \(2010a\)](#) given by

$$U(\eta, \nu, z) = -\frac{1}{\Gamma(\nu)} (\ln(z) + \psi(\eta) + 2\gamma) + \mathcal{O}(z \ln(z)), \quad \nu = 1,$$

where $\psi(\cdot), \gamma$ represent the digamma function and the Euler-Mascheroni constant respectively. Substituting $\eta = a_2 + 1/2, \nu = 3/2 - c_g$ and $z = \frac{t^2}{2}$ gives

$$U\left(a_2 + 1/2, 3/2 - c_g, \frac{t^2}{2}\right) = -\frac{1}{\Gamma(a_2 + 1/2)} \left(\ln\left(\frac{t^2}{2}\right) + \psi(a_2 + 1/2) + 2\gamma \right) + \mathcal{O}\left(t^2 \ln\left(\frac{t^2}{2}\right)\right), \quad c_g = 1/2.$$

The last expression is not defined at $t = 0$ and goes to infinity as $|t| \rightarrow 0$. To see the marginal priors are bounded when $c_g > 1/2$ it is sufficient to consider the cases given by equations 13.2.20-13.2.22 in [Olver et al. \(2010a\)](#) and making the proper substitutions of $\eta = a_2 + 1/2, \nu = 3/2 - c_g$ and $z = \frac{t^2}{2}$. In terms of the values c_g takes we have

$$U(\eta, \nu, t) \sim \begin{cases} \mathcal{O}(t^{2c_g-1}), & 1/2 < c_g < 3/2 \\ \mathcal{O}(t^2 \ln(t^2/2)), & c_g = 3/2 \\ \mathcal{O}(t^2), & c_g > 3/2 \end{cases}$$

The derivative of $U(\eta, \nu, z)$ is given by equation 13.3.22 in [Olver et al. \(2010a\)](#) as

$$\frac{d}{dz} U(\eta, \nu, z) = -\eta U(\eta + 1, \nu + 1, z).$$

Combining this with Equation (27) gives

$$\frac{d}{dz} U(\eta, \nu, z) = -\eta z^{-\nu} U(\eta - \nu + 1, 1 - \nu, z).$$

Substituting $\eta = a_2 + 1/2, \nu = 3/2 - c_g$ and $z = \frac{t^2}{2}$ results in

$$\frac{d}{dt}U\left(a_2 + 1/2, 3/2 - c_g, \frac{t^2}{2}\right) = Ct^{2c_g-2}U\left(a_2 + c_g, c_g - 1/2, \frac{t^2}{2}\right), \quad (28)$$

where $C = -(a_2 + 1/2)2^{3/2-c_g}$. Equation (28) is undefined at $t = 0$ when $c_g < 1$.
□

Proof of proposition 6

To prove the proposition we make use of Watson's lemma ([Miller, 2006](#)).

Proposition 11 (Watson's lemma). *Let $0 \leq T \leq \infty$ be fixed. Assume $f(t) = t^\lambda g(t)$, where $g(t)$ has an infinite number of derivatives in the neighborhood of $t = 0$, with $g(0) \neq 0$, and $\lambda > -1$. Suppose, in addition, either that $|f(t)| < Ke^{ct}$ for any $t > 0$, where K and c are independent of t . Then it is true that for all positive x that*

$$\left| \int_0^T e^{-xt} f(t) dt \right| < \infty$$

and that the following asymptotic equivalence holds:

$$\int_0^T e^{-xt} f(t) dt \sim \sum_{n=0}^{\infty} \frac{g^{(n)}(0) \Gamma(\lambda + n + 1)}{n! x^{\lambda+n+1}},$$

for $x > 0$ as $x \rightarrow \infty$.

The marginal distribution of a coefficient b is given by

$$\begin{aligned} p(b) &= \frac{1}{\sqrt{2\pi} B(c_g, a_2)} \int_0^\infty \exp\left\{-\frac{|b|^2}{2}t\right\} t^{\eta-1} (t+1)^{\nu-\eta-1} dt \\ &= \int_0^\infty \exp\{-zt\} f(t) dt, \end{aligned}$$

where $z = \frac{|b|^2}{2}$, $f(t) = Ct^{\eta-1}(t+1)^{\nu-\eta-1} = t^{\eta-1}g(t)$, $C = (\sqrt{2\pi}B(c_g, a_2))^{-1}$, and $g(t) = C(t+1)^{\nu-\eta-1}$. Setting $\lambda = \eta - 1$, the hypothesis $\lambda > -1$ is satisfied since $a_2 - 1/2 > -1$ for $a_2 > 0$. Moreover, $g(t)$ is infinitely differentiable around $t = 0$ and $g(0) = 0$. By Watson's Lemma, since $|f(t)| < Ke^{ct}$ for all $t > 0$ where K and c are independent of t , then as $|b| \rightarrow \infty$,

$$p(z|\sigma) = \sum_{n=0}^{\infty} \frac{g^{(n)}(0) \Gamma(\lambda + n + 1)}{n! z^{\lambda+n+1}}.$$

Truncating the sum at $n = 2$ gives

$$\begin{aligned} p(z) &= C \left\{ \frac{\Gamma(a_2 + 1/2)}{z^{a_2+1/2}} - \frac{(c_g + a_2)\Gamma(a_2 + 3/2)}{z^{a_2+3/2}} + \frac{(c_g + a_2)(c_g + a_2 + 1)\Gamma(a_2 + 5/2)}{z^{a_2+5/2}} \right\} \\ &\quad + \mathcal{O}\left(\frac{1}{z^{a_2+7/2}}\right) \\ &\sim \mathcal{O}\left(\frac{1}{z^{a_2+1/2}}\right). \end{aligned}$$

Therefore $p(|b|) \sim \mathcal{O}\left(\frac{1}{|b|^{2a_2+1}}\right)$. When $a_2 < 1/2$ as $|b| \rightarrow \infty$ and comparing with a Cauchy distribution represented by $\frac{1}{b^2}$, we have that

$$\frac{p(b)}{\frac{1}{b^2}} \sim \mathcal{O}\left(\frac{1}{b^{2a_2-1}}\right) \rightarrow \infty.$$

Proof of proposition 7

Since we have shown that $\lambda_{gl}^2 \sim \text{BetaPrime}(c_g, a_2)$, we can write the Therefore the Group-R2 prior can be written as

$$b_{gl} \mid \lambda_{gl}^2 \sim \text{Normal}(0, \lambda_{gl}), \quad \lambda_{gl}^2 \sim \text{BetaPrime}(c_g, a_2).$$

When $c_g = 1/2$ and $a_2 = \frac{1}{2}$, then $\lambda_{gl} \sim \text{Cauchy}^+(0, 1)$ and we have

$$b_{gl} \mid \lambda_{gl}^2 \sim \text{Normal}(0, \lambda_{gl}), \quad \lambda_{gl} \sim \text{Cauchy}^+(0, 1).$$

The horseshoe prior has the following representation ([Carvalho et al., 2010](#)):

$$b_{gl} \mid \lambda_{gl}, \omega \sim \text{Normal}(0, \lambda_{gl}\omega), \quad \lambda_{gl} \sim \text{Cauchy}^+(0, 1),$$

where λ_{gl} are per coefficient shrinkage parameters and ω is the global shrinkage parameter. Therefore the Group-R2 prior with $c_g = a_2 = \frac{1}{2}$ corresponds to a horseshoe prior with global scale $\omega = 1$. This proves the first part of the proposition.

To see that bounded influence holds, consider $y \mid b \sim \text{Normal}(b, 1)$, where we have dropped the index for notational convenience. [Carvalho et al. \(2010\)](#) shows that

$$\mathbb{E}(b \mid y^*) = y^* + \frac{d}{dy^*} \log m(y^*), \quad (29)$$

where $m(y^*)$ is the marginal density for y^* given by $m(y^*) = \int p(y^*|b)p(b)db$. [Carvalho et al. \(2010\)](#) further shows that as $|y^*| \rightarrow \infty$ then

$$\lim_{|y^*| \rightarrow \infty} \frac{d}{dy^*} \log m(y^*) = 0.$$

The specific form of $m(y^*)$ can be found and is given by

$$\begin{aligned} m(y^*) &= \frac{1}{(2\pi^3)^{1/2}} \int_0^\infty \exp\left(-\frac{y^{*2}/2}{1+\lambda^2}\right) \frac{1}{(1+\lambda^2)^{3/2}} d\lambda \\ &= \frac{1}{(2\pi^3)^{1/2}} \int_0^1 \exp(-1/2 y^{*2} z) z^{-1/2} dz \\ &= \frac{1}{\pi} \frac{\operatorname{erf}(y^*/\sqrt{2})}{y^*}, \end{aligned}$$

where we have used the change of variables $z = \frac{1}{\lambda^2+1}$. Here $\operatorname{erf}(\cdot)$ denotes the error function given by $\operatorname{erf}(x) = \frac{2}{\sqrt{\pi}} \int_0^x e^{-t^2} dt$ (Olver et al., 2010b). Therefore

$$\frac{d}{dy^*} \log m(y^*) = \frac{\sqrt{\frac{2}{\pi}} e^{-y^{*2}/2}}{\operatorname{erf}(y^*/\sqrt{2})} - \frac{1}{y^*},$$

and $\lim_{|y^*| \rightarrow \infty} \frac{d}{dy^*} \log m(y^*) = 0$. Using this and (29) shows that as $|y^*| \rightarrow \infty$ then $\mathbb{E}(b | y^*) \approx y^*$. \square

This implies that large signals become unregularized under the prior.

Proof of proposition 8

Denote by $b_g = (b_{g1}, \dots, b_{gp_g})'$ and $\Sigma_{b_g} = \tau^2 \operatorname{diag}\{\varphi_{g1}, \dots, \varphi_{gp_g}\}$. For a fixed group g , the joint distribution of $b_g | \tau_g^2, \varphi_g$ is

$$b_g | \tau_g^2, \varphi_g \sim \operatorname{Normal}(0, \Sigma_{b_g}).$$

We are interested in the distribution of $p(b_g | \varphi_g)$. This is given by

$$\begin{aligned} p(b_g | \varphi_g) &= \int_0^\infty p(b_g, \tau_g^2 | \varphi_g) d\tau_g^2 \\ &= \int_0^\infty p(b_g | \tau_g^2, \varphi_g) p(\tau_g^2) d\tau_g^2. \end{aligned}$$

For notational convenience we will use $t = \tau_g^2$. By hypothesis $\tau_g^2 \sim \operatorname{BetaPrime}(c_g, a_2)$, therefore

$$p(b_g | \varphi_g) = \int_0^\infty (2\pi)^{-p_g/2} |\Sigma_{b_g}|^{-1/2} \exp\left\{-\frac{1}{2} b_g' \Sigma_{b_g}^{-1} b_g\right\} \frac{1}{\operatorname{B}(c_g, b)} t^{c_g-1} (1+t)^{-c_g-b} dt$$

$$= \frac{(2\pi)^{-p_g/2} \left(\prod_{l=1}^{p_g} \varphi_{gl}\right)^{-1/2}}{B(c_g, a_2)} \int_0^\infty t^{c_g - p_g/2 - 1} (1+t)^{-c_g - a_2} \exp \left\{ -\frac{1}{2} \sum_{l=1}^{p_g} \frac{b_{gl}^2}{\varphi_{gl}} \frac{1}{t} \right\} dt$$

Setting $K = (2\pi)^{-p_g/2} \left(\prod_{l=1}^{p_g} \varphi_{gl}\right)^{-1/2} / B(c_g, a_2)$, $\alpha = c_g - p_g/2$, $\beta = c_g + a_2$, $\gamma = \sum_{l=1}^{p_g} \frac{b_{gl}^2}{\varphi_{gl}}$, and using the change of variable $u = 1/t$ gives

$$\begin{aligned} p(b_g \mid \varphi_g) &= K \int_0^\infty u^{\beta - \alpha - 1} (u+1)^{-\beta} \exp \{-\gamma/2\} du \\ &= K \Gamma(\beta - \alpha) U(\beta - \alpha, 1 - \alpha, \gamma/2) \\ &= \frac{(2\pi)^{-p_g/2} \left(\prod_{l=1}^{p_g} \varphi_{gl}\right)^{-1/2}}{B(c_g, a_2)} \Gamma(a_2 + p_g/2) U\left(a_2 + p_g/2, 1 + p_g/2 - c_g, \sum_{l=1}^{p_g} \frac{b_{gl}^2}{2\varphi_{gl}}\right). \end{aligned}$$

Using the identity (27) we have

$$p(b_g \mid \varphi_g) = \frac{(2\pi)^{-p_g/2} \left(\prod_{l=1}^{p_g} \varphi_{gl}\right)^{-1/2}}{B(c_g, a_2)} \Gamma(a_2 + p_g/2) \left(\frac{b_{gl}^2}{2\varphi_{gl}}\right)^{c_g - p_g/2} U\left(a_2 + c_g, 1 - p_g/2 + c_g, \sum_{l=1}^{p_g} \frac{b_{gl}^2}{2\varphi_{gl}}\right).$$

The right hand side has a singularity at the origin when $c_g < p_g/2$ and $b_{gl} \rightarrow 0$ for all $l = 1, \dots, p_g$. \square

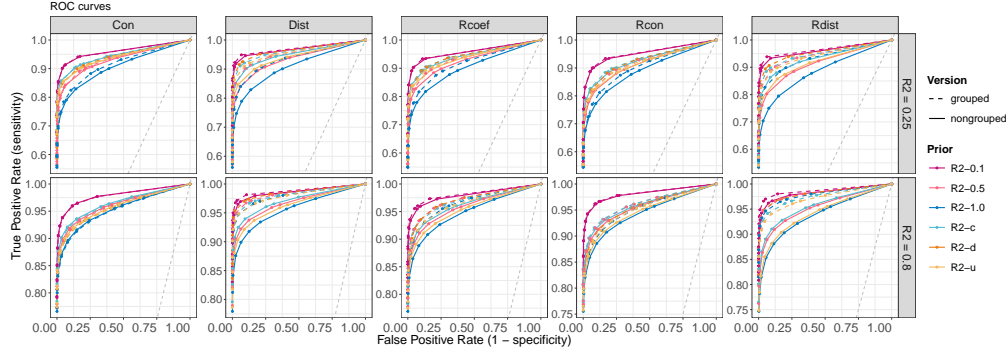


Figure 12: **ROC curves for the lower-dimensional scenario** ($p = 100, n = 200$). Grouped and non-grouped R^2 priors are compared. The grey line shows the diagonal of the unit square. “Con” denotes the concentrated signal, “Dist” the distributed signal, “Rcon” and “Rdist” their random counterparts, and “Rcoef” the random coefficients setting.

5.2 Experiments

In the following we present additional results for the simulations.

Simulations: Lower-dimensional results

Figure 12 displays ROC curves for the various priors across the considered low-dimensional scenarios. Overall, Group- R^2 priors tend to outperform their non-grouped counterparts, particularly in settings where the signal is concentrated within specific groups. For example, this advantage is clearly visible for the R^2 -1.0 prior, which shows consistently better performance across all data-generating processes. However, as the concentration parameter c_g decreases the performance gap narrows. For instance, under the R^2 -0.1 prior, the benefit of grouping becomes less pronounced.

Simulations: High-dimensional results

We present the partitioned ΔRMSE results in Figures 13 and 14, corresponding to truly zero and truly nonzero coefficients, respectively. The overall trends mirror those observed in the low-dimensional setting. Grouped versions of the R^2 prior consistently outperform their non-grouped counterparts in detecting noise, with the exception of the concentrated signal scenario. In terms of signal recovery, certain priors lead to improved performance. As discussed earlier, the uniform R^2 prior appears to offer a robust default across scenarios. However, we believe that incorporating well-informed prior knowledge about the grouping structure or sparsity pattern could lead to further gains.

Figure 15 shows the ROC curves for the high-dimensional case. The results again

parallel the low-dimensional setting: under high noise and sparse signals, grouping structures help distinguish signal from noise more accurately on average, improving overall classification performance.

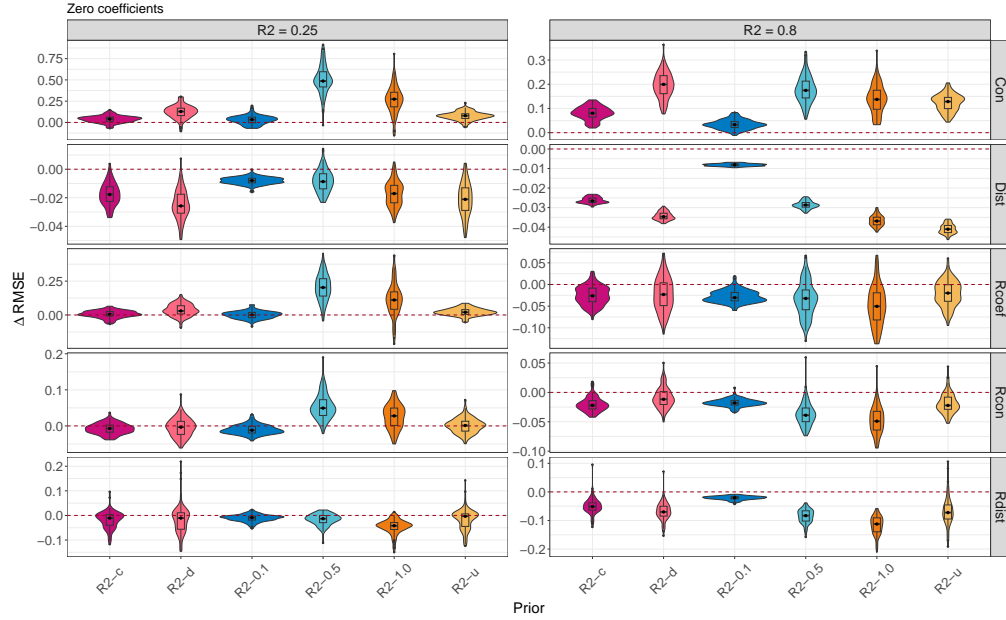


Figure 13: ΔRMSE for truly zero coefficients for the high-dimensional scenario ($p = 500$, $n = 200$). Values below the line indicate improvement in parameter recovery when considering groups. “Con” denotes the concentrated signal, “Dist” the distributed signal, “Rcon” and “Rdist” their random counterparts, and “Rcoef” the random coefficients setting.

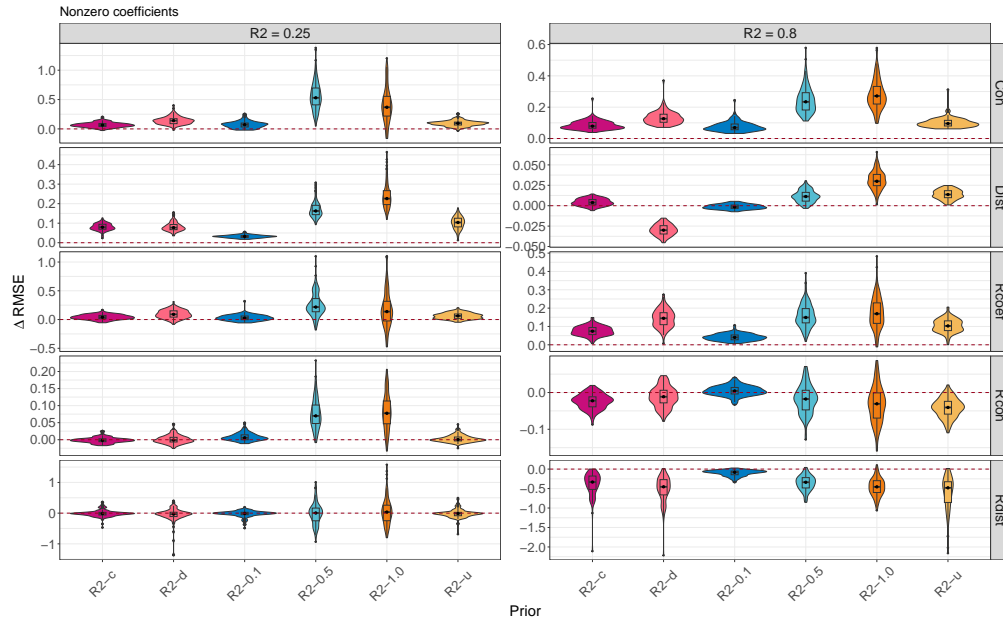


Figure 14: $\Delta RMSE$ for truly nonzero coefficients for the high-dimensional scenario ($p = 500$, $n = 200$). Values below the line indicate improvement in parameter recovery when considering groups. “Con” denotes the concentrated signal, “Dist” the distributed signal, “Rcon” and “Rdist” their random counterparts, and “Rcoef” the random coefficients setting.

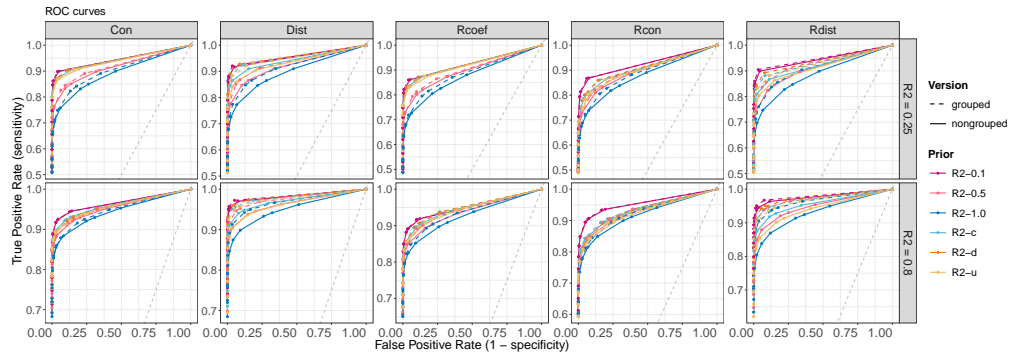


Figure 15: **ROC curves for the high-dimensional scenario** ($p = 500, n = 200$). Grouped and non-grouped R^2 priors are compared. The grey line shows the diagonal of the unit square. “Con” denotes the concentrated signal, “Dist” the distributed signal, “Rcon” and “Rdist” their random counterparts, and “Rcoef” the random coefficients setting.

References

- Aguilar, J. E. and Bürkner, P.-C. (2025). “Dependency-Aware Shrinkage Priors for High Dimensional Regression.” *arXiv preprint arXiv:2505.10715*. 15
- Aguilar, J. E. and Bürkner, P.-C. (2023). “Intuitive joint priors for Bayesian linear multilevel models: The R2D2M2 prior.” *Electronic Journal of Statistics*, 17(1): 1711 – 1767.
URL <https://doi.org/10.1214/23-EJS2136> 1, 5, 17
- (2025). “Generalized Decomposition Priors on R2.” *Bayesian Analysis*, 1 – 34.
URL <https://doi.org/10.1214/25-BA1524> 1, 5, 9
- Aguilar, J. E., Kohns, D., Vehtari, A., and Bürkner, P.-C. (2025). “Supplement to ”R2 priors for Grouped Variance Decomposition in High-dimensional Regression”.” 8
- Aitchison, J. and Shen, S. M. (1980). “Logistic-Normal Distributions: Some Properties and Uses.” *Biometrika*, 67(2): 261–272.
URL <http://www.jstor.org/stable/2335470> 5
- Aitchison, J. J. (1986). *The statistical analysis of compositional data / J. Aitchison..* Monographs on statistics and applied probability (Series). Chapman and Hall. 5
- Armagan, A., Dunson, D. B., Lee, J., Bajwa, W. U., and Strawn, N. (2013). “Posterior consistency in linear models under shrinkage priors.” *Biometrika*, 100(4): 1011–1018.
URL <https://doi.org/10.1093/biomet/ast028> 12
- Bai, R. and Ghosh, M. (2019). “Large-scale multiple hypothesis testing with the normal-beta prime prior.” *Statistics*, 53(6): 1210–1233.
URL <https://doi.org/10.1080/02331888.2019.1662017> 13
- (2021). “On the Beta Prime Prior for Scale Parameters in High-Dimensional Bayesian Regression Models.” *Statistica Sinica*.
URL <http://arxiv.org/abs/1807.06539> 4, 11
- Benjamini, Y. and Hochberg, Y. (1995). “Controlling the False Discovery Rate: A Practical and Powerful Approach to Multiple Testing.” *Journal of the Royal Statistical Society. Series B (Methodological)*, 57(1): 289–300.
URL <http://www.jstor.org/stable/2346101> 19
- Bentler, P. M. and Bonett, D. G. (1980). “Significance tests and goodness of fit in the analysis of covariance structures.” *Psychological Bulletin*, 88(3): 588–606. Place: US Publisher: American Psychological Association. 1
- Bhattacharya, A., Pati, D., Pillai, N. S., and Dunson, D. B. (2015). “Dirichlet–Laplace Priors for Optimal Shrinkage.” *Journal of the American Statistical Association*, 110(512): 1479–1490.
URL <https://doi.org/10.1080/01621459.2014.960967> 5, 11
- Boss, J., Datta, J., Wang, X., Park, S. K., Kang, J., and Mukherjee, B. (2023). “Group Inverse-Gamma Gamma Shrinkage for Sparse Linear Models with Block-Correlated Regressors.” *Bayesian Analysis*, 1 – 30.
URL <https://doi.org/10.1214/23-BA1371> 2, 6, 7, 12, 17, 19, 22

- Brooks, Gelman, S., and Jones, A. (2011). *Handbook of Markov Chain Monte Carlo*. Chapman and Hall/CRC, 1 edition. 18, 19
- Carpenter, B., Gelman, A., Hoffman, M. D., Lee, D., Goodrich, B., Betancourt, M., Brubaker, M., Guo, J., Li, P., and Riddell, A. (2017). “Stan: A Probabilistic Programming Language.” *Journal of Statistical Software*, 76(1): 1–32.
URL <https://www.jstatsoft.org/index.php/jss/article/view/v076i01> 17
- Carvalho, C. M., Polson, N. G., and Scott, J. G. (2009). “Handling Sparsity via the Horseshoe.” In van Dyk, D. and Welling, M. (eds.), *Proceedings of the Twelfth International Conference on Artificial Intelligence and Statistics*, volume 5 of *Proceedings of Machine Learning Research*, 73–80. PMLR.
URL <https://proceedings.mlr.press/v5/carvalho09a.html> 7
- (2010). “The horseshoe estimator for sparse signals.” *Biometrika*, 97(2): 465–480.
URL <http://www.jstor.org/stable/25734098> 11, 12, 33
- Castillo, I., Schmidt-Hieber, J., and van der Vaart, A. (2015). “Bayesian Linear Regression with Sparse Priors.” *The Annals of Statistics*, 43(5): 1986–2018.
URL <https://www.jstor.org/stable/43818568> 13
- Castillo, I. and Vaart, A. v. d. (2012). “Needles and Straw in a Haystack: Posterior concentration for possibly sparse sequences.” *The Annals of Statistics*, 40(4): 2069 – 2101.
URL <https://doi.org/10.1214/12-AOS1029> 13
- Coelho, C. A. and Alberto, R. P. (2021). “On the Distribution of the Product of Independent Beta Random Variables — Applications.” In Ghosh, I., Balakrishnan, N., and Ng, H. K. T. (eds.), *Advances in Statistics - Theory and Applications: Honoring the Contributions of Barry C. Arnold in Statistical Science*, 85–117. Cham: Springer International Publishing.
URL https://doi.org/10.1007/978-3-030-62900-7_5 9
- Gelman, A. (2006). “Prior distributions for variance parameters in hierarchical models (comment on article by Browne and Draper).” *Bayesian Analysis*, 1(3): 515 – 534.
URL <https://doi.org/10.1214/06-BA117A> 6
- Gelman, A., Carlin, J., Stern, H., Dunson, D., Vehtari, A., and Rubin, D. (2013). *Bayesian Data Analysis, Third Edition*. Chapman & Hall/CRC Texts in Statistical Science. Taylor & Francis. 1
- Goodrich, B., Gabry, J., Ali, I., and Brilleman, S. (2020). “rstanarm: Bayesian applied regression modeling via Stan.”
URL <https://mc-stan.org/rstanarm> 6
- Hoffman, M. D. and Gelman, A. (2014). “The No-U-Turn Sampler: Adaptively Setting Path Lengths in Hamiltonian Monte Carlo.” *J. Mach. Learn. Res.*, 15(1): 1593–1623. 18
- Jeffrey, A., Zwillinger, D., Gradshteyn, I., and Ryzhik, I. (2007). “8–9 - Special Functions.” In *Table of Integrals, Series, and Products (Seventh Edition)*, 859–1048.

- Boston: Academic Press, seventh edition edition.
 URL <https://www.sciencedirect.com/science/article/pii/B9780080471112500169> 11, 14, 30
- Kohns, D., Kallioinen, N., McLatchie, Y., and Vehtari, A. (2025). “The ARR2 Prior: Flexible Predictive Prior Definition for Bayesian Auto-Regressions.” *Bayesian Analysis*, 1 – 32.
 URL <https://doi.org/10.1214/25-BA1512> 1, 5
- Kohns, D. and Potjagailo, G. (2025). “Flexible Bayesian MIDAS: time-variation, group-shrinkage and sparsity.” *Journal of Business & Economic Statistics*, 1–17. 1
- Li, C. and Li, H. (2008). “Network-constrained regularization and variable selection for analysis of genomic data.” *Bioinformatics*, 24(9): 1175–1182.
 URL <https://doi.org/10.1093/bioinformatics/btn081> 1
- Lin, J. (2016). “On The Dirichlet Distribution by Jiayu Lin.” 5, 17, 28
- Miller, P. (2006). *Applied Asymptotic Analysis*. American Mathematical Society, 1 edition. 32
- Müller, P. and Quintana, F. A. (2004). “Nonparametric Bayesian Data Analysis.” *Statistical Science*, 19(1): 95 – 110.
 URL <https://doi.org/10.1214/088342304000000017> 3
- Neal, R. M. (2011). *MCMC using Hamiltonian dynamics*.
 URL <http://arxiv.org/abs/1206.1901> 18
- Olver, F., of Standards, N. I., (U.S.), T., Lozier, D., Boisvert, R., and Clark, C. (2010a). *NIST Handbook of Mathematical Functions Hardback and CD-ROM*. Cambridge University Press.
 URL <https://books.google.de/books?id=3I15Ph1Qf38C> 30, 31
- Olver, F., Standards, N. I. o., (U.S.), T., Lozier, D., Boisvert, R., and Clark, C. (2010b). *NIST Handbook of Mathematical Functions Hardback and CD-ROM*. Cambridge University Press. 11, 29, 34
- Pas, S. L. v. d. (2021). “Theoretical guarantees for the horseshoe and other global-local shrinkage priors.” In *Handbook of Bayesian Variable Selection*, 133–160. Chapman and Hall/CRC. 11, 12
- Pas, S. L. v. d., Kleijn, B. J. K., and Vaart, A. W. v. d. (2014). “The horseshoe estimator: Posterior concentration around nearly black vectors.” *Electronic Journal of Statistics*, 8(2): 2585 – 2618.
 URL <https://doi.org/10.1214/14-EJS962> 11, 13
- Pas, S. L. v. d., Salomond, J.-B., and Schmidt-Hieber, J. (2016). “Conditions for posterior contraction in the sparse normal means problem.” *Electronic Journal of Statistics*, 10(1): 976 – 1000.
 URL <https://doi.org/10.1214/16-EJS1130> 12, 13
- Pas, S. L. v. d., Szabó, B., and Vaart, A. v. d. (2017). “Uncertainty Quantification for

- the Horseshoe (with Discussion).” *Bayesian Analysis*, 12(4): 1221 – 1274.
URL <https://doi.org/10.1214/17-BA1065> 11
- Piironen, J. and Vehtari, A. (2017). “Sparsity information and regularization in the horseshoe and other shrinkage priors.” *Electronic Journal of Statistics*, 11(2): 5018 – 5051.
URL <https://doi.org/10.1214/17-EJS1337SI> 12, 14, 15
- Robert, C. (2007). *The Bayesian Choice: From Decision-Theoretic Foundations to Computational Implementation*. Springer Texts in Statistics. Springer New York. 18
- Schmidt, D. F. and Makalic, E. (2020). “Log-Scale Shrinkage Priors and Adaptive Bayesian Global-Local Shrinkage Estimation.”
URL <https://arxiv.org/abs/1801.02321> 5, 9
- Schmüdgen, K. (2020). “Ten Lectures on the Moment Problem.” ArXiv:2008.12698 [math].
URL <http://arxiv.org/abs/2008.12698> 9
- Stan Development Team (2024). “Stan Modeling Language Users Guide and Reference Manual, Version 2.36.”
URL <http://mc-stan.org/> 17
- Sun, H., Lin, W., Feng, R., and Li, H. (2014). “NETWORK-REGULARIZED HIGH-DIMENSIONAL COX REGRESSION FOR ANALYSIS OF GENOMIC DATA.” *Statistica Sinica*, 24(3): 1433–1459. 1
- Tew, S. Y., Schmidt, D. F., and Boley, M. (2025). “GRASP: Grouped Regression with Adaptive Shrinkage Priors.”
URL <https://arxiv.org/abs/2506.18092> 9, 10
- Vehtari, A., Gelman, A., and Gabry, J. (2016). “Practical Bayesian model evaluation using leave-one-out cross-validation and WAIC.” *Statistics and Computing*, 27(5): 1413–1432.
URL <http://dx.doi.org/10.1007/s11222-016-9696-4> 18
- Vehtari, A., Gelman, A., Simpson, D., Carpenter, B., and Bürkner, P.-C. (2021). “Rank-Normalization, Folding, and Localization: An Improved \hat{R} for Assessing Convergence of MCMC (with Discussion).” *Bayesian Analysis*, 16(2): 667 – 718.
URL <https://doi.org/10.1214/20-BA1221> 19
- Vehtari, A. and Ojanen, J. (2012). “A survey of Bayesian predictive methods for model assessment, selection and comparison.” *Statistics Surveys*, 6(none): 142 – 228.
URL <https://doi.org/10.1214/12-SS102> 18
- Xu, X. and Ghosh, M. (2015). “Bayesian Variable Selection and Estimation for Group Lasso.” *Bayesian Analysis*, 10(4).
URL <https://projecteuclid.org/journals/bayesian-analysis/volume-10/issue-4/Bayesian-Variable-Selection-and-Estimation-for-Group-Lasso/10.1214/14-BA929.full> 2
- Xu, Z., Schmidt, D. F., Makalic, E., Qian, G., and Hopper, J. L. (2016). “Bayesian

- Grouped Horseshoe Regression with Application to Additive Models.” In Kang, B. H. and Bai, Q. (eds.), *AI 2016: Advances in Artificial Intelligence*, Lecture Notes in Computer Science, 229–240. Cham: Springer International Publishing. 2
- Yanchenko, E., Bondell, H. D., and and, B. J. R. (2025a). “The R2D2 Prior for Generalized Linear Mixed Models.” *The American Statistician*, 79(1): 40–49.
URL <https://doi.org/10.1080/00031305.2024.2352010> 1
- Yanchenko, E., Irie, K., and Sugasawa, S. (2025b). “The Group R2D2 Shrinkage Prior for Sparse Linear Models with Grouped Covariates.”
URL <https://arxiv.org/abs/2412.15293> 7
- Zhang, Y. D., Naughton, B. P., Bondell, H. D., and Reich, B. J. (2020). “Bayesian Regression Using a Prior on the Model Fit: The R2-D2 Shrinkage Prior.” *Journal of the American Statistical Association*, 0(0): 1–13.
URL <https://doi.org/10.1080/01621459.2020.1825449> 1, 5, 28